\$50 CH ELSEVIER Contents lists available at ScienceDirect

Journal of Computational and Applied Mathematics

journal homepage: www.elsevier.com/locate/cam



A robust numerical integrator for the short pulse equation near criticality



S. Sato^{a,*}, K. Oguma, T. Matsuo^a, B.-F. Feng^b

- ^a Graduate School of Information Science and Technology, The University of Tokyo, Bunkyo-ku, Tokyo, Japan
- ^b School of Mathematical and Statistical Sciences, The University of Texas Rio Grande Valley, Edinburg, TX, USA

ARTICLE INFO

Article history: Received 6 May 2018 Received in revised form 27 January 2019

MSC: 65M06 78A60

Keywords: Short pulse equation Sine-Gordon equation Hodograph transformation Self-adaptive moving mesh Discrete conservation law

ABSTRACT

The short pulse equation was introduced by Schäfer–Wayne (2004) for modeling the propagation of ultrashort optical pulses. While it can describe a wide range of solutions, its ultrashort pulse solutions with a few cycles, which the conventional nonlinear Schrödinger equation does not possess, have drawn much attention. In such a region, the solutions can become quite close to a singularity, and thus existing numerical methods cease to work stably, or even if they do, they require high computational cost. In this paper, we propose a robust numerical integration method which is obtained by combining a hodograph transformation and some structure-preserving methods. The resulting scheme successfully works even when the singularity occurs, and thus gives a highly robust method for resolving near singular solutions of interest. It is confirmed by numerical experiments, and some new insights about derivative blow-up are obtained.

© 2019 Elsevier B.V. All rights reserved.

1. Introduction

In this paper, we consider the numerical integration of the short pulse (SP) equation

$$u_{tx} = u + \frac{1}{6} \left(u^3 \right)_{xx},$$
 (1)

which is a model equation of ultrashort optical pulses in nonlinear media [1,2]. Here, $t \in \mathbb{R}_+ := [0, +\infty)$ and $x \in \mathbb{R}$ denote temporal and spatial independent variables, respectively. The dependent variable u = u(t, x) represents the magnitude of the electric field, and subscripts t and x denote partial differentiations. Although this equation is usually considered on the whole real line \mathbb{R} with the vanishing boundary condition $|u(t, x)| \to 0$ as $|x| \to \infty$, in this paper, for the consistency with numerical treatment, we consider the problem on the circle, i.e., under the periodic boundary condition u(t, x+L) = u(t, x) for any $t \in \mathbb{R}_+$ and $x \in \mathbb{R}$, where $t \in \mathbb{R}_+$ is a constant representing the length of the period.

We here summarize the theoretical results obtained so far, most of which were established on \mathbb{R} . Brunelli [3,4] found its hierarchy and bi-Hamiltonian structure. Sakovich–Sakovich [5] proved the integrability of the SP equation by showing that it is associated with the sine-Gordon (SG) equation in light-cone coordinates

$$\theta_{rs} = \sin \theta$$
 (2)

via a hodograph transformation. Here, τ and s denote new temporal and spatial independent variables. It was then shown that breather soliton solutions of the SP equation can be generated from those of the SG equation [6]. Another interesting

E-mail addresses: shun_sato@mist.i.u-tokyo.ac.jp (S. Sato), matsuo@mist.i.u-tokyo.ac.jp (T. Matsuo), baofeng.feng@utrgv.edu (B.-F. Feng).

^{*} Corresponding author.

outcome of this SG formulation is that wide range of multi-valued, exotic solutions such as loop solutions can be regarded as the solutions of the SP equation; see, for example, [7–11]. From the theoretical aspects as the partial differential equation (PDE), the global well-posedness of the SP equation (and the SG equation) was discussed by Pelinovsky–Sakovich [12], whereas the local well-posedness was already proved by Schäfer–Wayne [1]. A similar result for entropy solutions was recently shown by Coclite–di Ruvo [13] (see, also [14]). On the other hand, Liu–Pelinovsky–Sakovich [15] found the conditions of the wave breaking in the SP equation (see also Sakovich [16]). Some generalizations of the SP equation have been considered as well, including vector SP equation [17], regularized SP equation [18], integrable coupled SP equation [19], higher-order SP equation [20], stochastic SP equation [21], and (coupled) complex SP equation [22]. There are also a few results for the circle (periodic) case. Parkes [23] and Matsuno [24] found various periodic solutions (see, also [25]). Liu–Pelinovsky–Sakovich [15] also dealt with local well–posedness and wave breaking scenario on the circle.

When it comes to its numerical treatment, surprisingly, it seems much less have been understood. Sakovich [16] employed the Fourier-spectral and Runge–Kutta methods to verify the well-posedness and wave-breaking of the SP equation. Pietrzyk–Kanattšikov [26] applied a multi-symplectic integrator for the SP equation, and concluded that the multi-symplectic integrator is more efficient than Fourier-spectral methods. Recently, Coclite–Ridder–Risebro [14] extended standard monotone finite difference schemes for conservation laws, and showed that the numerical solution converges to the unique entropy solution (note that their method and analysis are applicable to any equations in the form $u_{tx} = u + (f(u))_{xx}$, where $f \in C^2(\mathbb{R})$).

One reason for the lack of numerical studies perhaps lies in the fact that the SP equation intrinsically aims at (nearly) singular solutions. Let us describe the situation taking the typical pulse solution on \mathbb{R} devised in [6]:

$$\begin{cases} u(\tau, s) = 4\xi \zeta \frac{\xi \sin \psi \sinh \phi + \zeta \cos \psi \cosh \phi}{\xi^2 \sin^2 \psi + \zeta^2 \cosh^2 \phi}, \\ x(\tau, s) = s + 2\xi \zeta \frac{\xi \sin 2\psi - \zeta \sinh 2\phi}{\xi^2 \sin^2 \psi + \zeta^2 \cosh^2 \phi}. \end{cases}$$
(3)

The parameter $\xi \in (0, 1)$ determines the shape of the wave, and other parameters are defined as

$$\zeta := \sqrt{1 - \xi^2}, \quad \phi := \xi(s + \tau), \quad \psi := \zeta(s - \tau).$$

This solution with $\xi < \xi_{cr} = \sin{(\pi/8)} \approx 0.383$ is nonsingular, whereas the singularities $u_x \to \pm \infty$ appear when $\xi \ge \xi_{cr}$ (see Fig. 1 for the shape of the solution); beyond the *critical* value, the solution becomes multi-valued, and only of mathematical interest. According to our preliminary numerical tests, existing numerical methods can handle nonsingular solutions far enough away from the threshold ξ_{cr} . As ξ approaches to the criticality, however, those numerical methods become quite unstable, and require very small mesh sizes and accordingly high computational cost to resolve the phenomena near criticality. This is a serious problem if we recall what the SP equation is for—it aims at capturing ultrashort optical pulses with only a few oscillations of the electric field. The rapid development of laser technologies enabled the actual generation of such ultrashort pulses. In such a region, the standard nonlinear Schrödinger equation, which assumes slowly varying amplitude, does not give an accurate approximation, and that is exactly the situation the SP equation is designed for (see [27–30] for other studies on modeling few-cycle pulses). In fact, one may check the original paper (Figure 4 in [1]) to find that the main focus is on the extreme case where only three or four visible peaks are in a single pulse (see also Figures 2 and 3 in [2]).

Let us illustrate the situation in terms of the solution (3), where ξ is taken to 0.38, which is a typical subcritical situation. For this nearly singular solution, let us, for example, see a result by a special numerical integrator that keeps an invariant of the SP equation (formulated in Section 4.1). Such a conservative method is generally believed to give qualitatively better results than generic methods for numerically tough problems, but unfortunately this is not the case here; see Fig. 1. There, results for four different meshes are shown. The coarsest case, (a) (where the spatial domain is divided into K = 255 grids, and the time step size Δt is taken to 0.1), clearly shows unphysical numerical oscillations. This does not improve by refining the time grid (the case (b)). By refining the spatial grid, it slightly improves (the case (c) and (d)), but we still observe the oscillations persist there. This means that in order to resolve such nearly singular solutions we need extremely fine meshes, and accordingly, high computational cost, even if we use a good structure-preserving method. This motivates us to turn to other directions. (Notice also that in Fig. 1 we find that the robust scheme proposed in this paper later works very well for the subcritical solution.)

Generally speaking, a good approach to treat such a localized, nearly singular solutions is to employ the *moving mesh methods* (see, e.g., [31,32]). In a moving mesh method [31], first the original PDE on u(t,x) is transformed to a parametrized form on, say, $u(\tau,s)$ and $x(\tau,s)$ (τ,s are new independent variables that replace t,x), and it is solved with a "moving mesh PDE" on $x(\tau,s)$ that describes the moving mesh strategy. Although this approach is quite effective in many problems, its direct application to the SP equation seems not adequate. The difficulty arises from the term u_{tx} , which implicitly casts a constraint $\int_0^t u(t,x) dx = 0$ (see, for example, Horikis [33]) on all solutions; this can be easily seen by integrating the SP equation. Although this linear constraint can be satisfied by simple methods (for example, the Fourier-spectral method [16]), it is generally lost when we incorporate a moving mesh mechanism. In fact, to the best of the authors' knowledge, there have been no moving mesh schemes for the PDEs of the form $u_{tx} = f(t,u)$ in the literature, which should be attributed to the observation above.

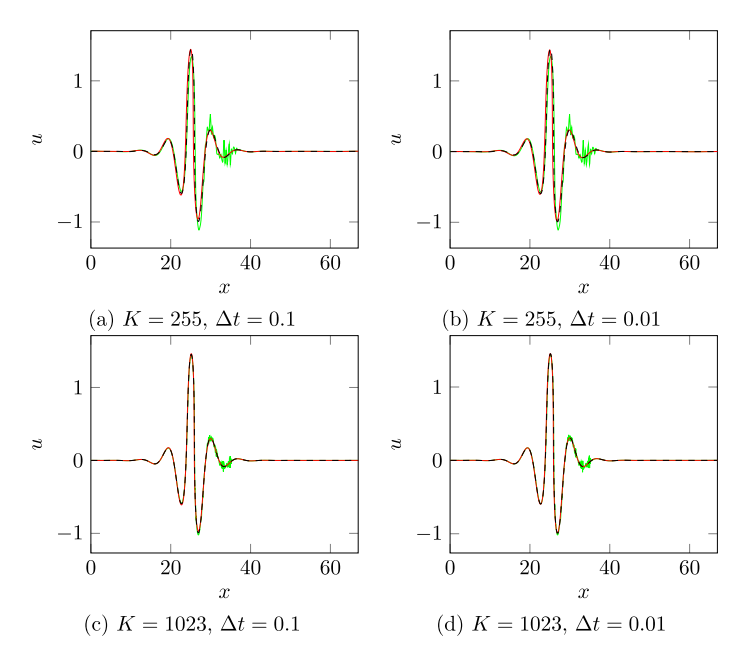


Fig. 1. Numerical solutions at T = 10 under each condition ((a), (b), (c), and (d)) for the initial data corresponding to (3) with $\xi = 0.38$. Solid lines in red and green are numerical solutions of the proposed scheme and the standard norm-preserving scheme, respectively. The dashed black line is the exact solution (3). (For interpretation of the references to color in this figure legend, the reader is referred to the web version of this article.)

In this paper, we thus further incorporate a technique from the research field of integrable systems, which is called *hodograph transformation*. Feng et al. [34] constructed an integrable discretization of the SP equation by utilizing the fact that the SP equation is related to the SG equation by the hodograph transformation. They started with a known integrable discretization of the SG equation, and by translating it with a discrete hodograph transformation, achieved a new integrable discretization of the SP equation. (Feng et al. [34] also dealt with the Wadati–Konno–Ichikawa elastic beam equation [35] and the complex Dym equation; see also [36–41].) Although these studies were successful as integrable systems studies, they themselves did not give any numerical integrators since (i) the works above mainly focused on the discrete reproduction of the solitons, and it was not clear how general initial data could be treated, and (ii) they considered problems only on \mathbb{R} , and the treatment of boundaries was set outside off their scope.

In this paper, by combining the above two ideas, we provide a new robust integrator for the SP equation. This combination requires, however, very delicate discussions so that the overall procedure gives a meaningful integrator, and that part is the main contribution of the present paper. The resulting scheme has the following advantages:

- (i) it can deal with arbitrary initial conditions, i.e., serves as an numerical integrator,
- (ii) it can run on the periodic boundary condition setting,
- (iii) the scheme can deal with even multi-valued solutions as well; as its practical consequence, it beautifully works also for physical solutions near criticality, and
- (iv) it is as a result a self-adaptive moving mesh scheme, i.e., the grids distribute appropriately without using an extra mesh PDE,

The rest of the present paper is organized as follows. In Section 2, we review and discuss the relation between the SP and the SG equations. Some facts are from the literature, but we will carry out our argument more carefully clarifying the treatment of the boundaries. Section 3 is devoted to the proposed scheme for the SP equation on the periodic domain. Then, we show the superiority of our proposed method by numerical experiments in Section 4. Finally, Section 5 is devoted to some concluding remarks.

2. Relating the SP equation to the SG equation: continuous case

In this section, we summarize some facts about the SP and the SG equations; although all of them are necessary for our numerical integrator, since it is a bit lengthy, one might hope to first see the scheme itself in Section 3, and come back to find necessary information accordingly.

We first start with pointing out some properties of the SP equation in Section 2.1. In Section 2.2, we discuss the transformation between the SP and the SG equations, and state exactly in which sense they are equivalent. Then Section 2.3 is devoted to the proof of an important, non-trivial fact that the physical and computational spaces can be

fixed in our regime. Up to this point, we leave the boundary condition open, so that the mathematical results so far are applicable to general cases other than the periodic boundary condition. In Section 2.4, we focus on the circle case, and show how we can treat the periodic boundary condition. Finally, in Section 2.5, we show our framework successfully recovers the implicit constraint of the SP equation, which completes the whole picture.

2.1. The SP equation: its conservation law and Hamiltonian structures

We start by reviewing a certain conservation law that will play an essential role in the following discussion. More precisely, the solution of the SP equation (1) preserves the "total arc-length" [3].

Let us consider the SP equation on a fixed physical domain [0, L] (we leave the boundary condition open for the moment). For a smooth function $u:[0, L] \to \mathbb{R}$, the total arc-length S(u) is defined as

$$S(u) := \int_0^L \sqrt{1 + (u_x(x))^2} dx.$$

For a function $u: \mathbb{R}_+ \times [0, L] \to \mathbb{R}$ and $t \in \mathbb{R}_+$, the notation $u(t): [0, L] \to \mathbb{R}$ denotes a function satisfying (u(t))(x) = u(t, x) for any $x \in [0, L]$. As shown in the following proposition, the total arc length S(u(t)) of a solution u of the SP equation (1) is invariant under certain boundary conditions.

Proposition 1. Let $u: \mathbb{R}_+ \times [0, L] \to \mathbb{R}$ be a smooth solution of the short pulse equation (1) with a boundary condition satisfying

$$\left[\frac{(u(t,x))^2 \sqrt{1 + (u_x(t,x))^2}}{2} \right]^L = 0.$$

Then, (d/dt)S(u(t)) = 0 holds for any $t \in \mathbb{R}_+$.

Proof. This proposition can be shown straightforwardly:

$$\begin{split} \frac{\mathrm{d}}{\mathrm{d}t} S(u(t)) &= \int_0^L \frac{\partial}{\partial t} \sqrt{1 + u_x^2} \mathrm{d}x = \int_0^L \frac{u_x}{\sqrt{1 + u_x^2}} u_{tx} \mathrm{d}x \\ &= \int_0^L \frac{u_x}{\sqrt{1 + u_x^2(t, x)}} \left(u + \frac{1}{6} \left(u^3 \right)_{xx} \right) \mathrm{d}x = \left[\frac{u^2 \sqrt{1 + u_x^2}}{2} \right]_0^L = 0. \end{split}$$

The last equality holds due to the assumption on the boundary condition. \Box

We also recall the fact that the SP equation has the bi-Hamiltonian structure (they are slight modifications of those given in [4]):

$$u_{t} = \left(\partial_{x}^{-1} + \frac{1}{8}(u^{2}\partial_{x} + \partial_{x}u^{2})\right) \frac{\delta \mathcal{I}}{\delta u}, \qquad \qquad \mathcal{I}(u) = \frac{1}{2} \int_{0}^{L} u^{2} dx, \qquad (4)$$

$$u_{t} = \partial_{x} \frac{\delta \mathcal{E}}{\delta u}, \qquad \qquad \mathcal{E}(u) = \int_{0}^{L} \left(\frac{1}{24}u^{4} - \frac{1}{2}\left(\partial_{x}^{-1}u\right)^{2}\right) dx,$$

where ∂_{ν}^{-1} is the antiderivative

$$\partial_x^{-1} v(x) = \int_0^x v(y) dy - \frac{1}{L} \int_0^L \int_0^z v(y) dy dz,$$

which is employed by Hunter [42] for the short wave equation (this can also be regarded as a generalized inverse of ∂_x , see e.g. [43]).

2.2. Transformation from the SP equation to the SG equation

Now let us discuss how we transform the SP equation to the SG equation. The transformation starts with the standard procedure in the moving mesh methods (see, for example, [31]). We introduce new space and time variables $s \in [0, S]$ and $\tau \in \mathbb{R}_+$, (τ actually coincides with t, but it is introduced here for the ease of handling independent variables). For the moment, S is assumed to be some constant, and later it will be redefined (see Fig. 2 and its explanation). The differential operators $\partial/\partial x$ and $\partial/\partial t$ can be replaced with $\partial/\partial s$ and $\partial/\partial \tau$ using the identities

$$\frac{\partial}{\partial x} = \frac{1}{x_s} \frac{\partial}{\partial s}, \qquad \qquad \frac{\partial}{\partial t} = \frac{\partial}{\partial \tau} - \frac{x_\tau}{x_s} \frac{\partial}{\partial s}.$$

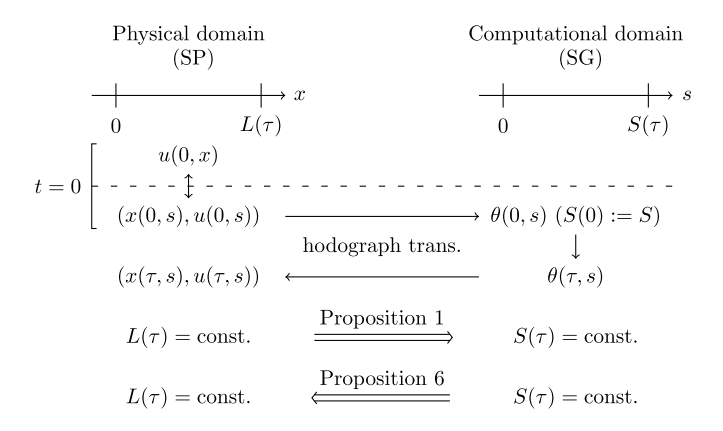


Fig. 2. The diagram of our strategy for self-adaptive moving mesh integration.

Then the SP equation (1) is transformed to

$$\left(\frac{1}{x_s}\frac{\partial}{\partial s}\right)\left(\frac{\partial}{\partial \tau} - \frac{x_\tau}{x_s}\frac{\partial}{\partial s}\right)u = u + \frac{1}{6}\left(\frac{1}{x_s}\frac{\partial}{\partial s}\right)^2 u^3,$$

which can be further simplified into

$$x_{s} (u_{\tau s} x_{s} - x_{\tau s} u_{s}) = u x_{s} \left(x_{s}^{2} + u_{s}^{2}\right) + \left(x_{\tau} + \frac{u^{2}}{2}\right) (u_{ss} x_{s} - x_{ss} u_{s})$$
(5)

by simple calculus. We call Eq. (5) a "parametrized form" of the SP equation. We call the solution of (5) as the solution curve of the SP equation by convention.

Remark 1. Since all strong solutions of the original SP equation (1) solves the parametrized form of the SP equation, this extension of the concept of the solution is quite natural. It should be noted that the pulse solution (3) in Introduction is the solution of the SP equation in this sense.

Another note should go to the fact that this extension gives way to extend the solution after the wave breaking (recall that Liu-Pelinovsky–Sakovich [15] proved that the wave breaking occurs for initial conditions satisfying a criterion). Sections 4.3 and 4.4 are devoted to a numerical experiment of the wave breaking and the behavior after the wave breaking.

Now we here start something different from the standard moving mesh approach. We regard the variable s as the "arc-length" of the solution u(t, x), and employ the hodograph transformations below [5]:

$$\begin{bmatrix} x(\tau,s) \\ u(\tau,s) \end{bmatrix} = \begin{bmatrix} x(\tau,0) \\ u(\tau,0) \end{bmatrix} + \int_0^s \begin{bmatrix} \cos\theta(\tau,\sigma) \\ \sin\theta(\tau,\sigma) \end{bmatrix} d\sigma, \tag{6a}$$

$$\begin{bmatrix} x_s(\tau, s) \\ u_s(\tau, s) \end{bmatrix} = \begin{bmatrix} \cos \theta(\tau, s) \\ \sin \theta(\tau, s) \end{bmatrix}. \tag{6b}$$

The hodograph transformation connects the expression $(x(\tau,s),u(\tau,s))$ in the two dimensional Cartesian coordinates with another expression in terms of the argument $\theta(\tau,s)$. Computing $\theta(\tau,s)$ from $(x(\tau,s),u(\tau,s))$ can be done by (6b). However, we need the "base point" $(x(\tau,0),u(\tau,0))$ when we compute $(x(\tau,s),u(\tau,s))$ back from $\theta(\tau,s)$. Notice that there remains a degree of freedom in choosing such a base point.

Let us relate the SP equation to the SG equation using the new variables. For any solution $(x(\tau, s), u(\tau, s))$ of the parametrized form (5) of the SP equation, by substituting (6), we obtain

$$(\theta_{\tau} - u)\cos\theta = \left(x_{\tau} + \frac{u^2}{2}\right)\theta_{s}.\tag{7}$$

Note that the relation above is equivalent to Eq. (5). By differentiating (7) with respect to s, we have

$$(\theta_{\tau s} - \sin \theta) \cos \theta = \left(x_{\tau} + \frac{u^2}{2}\right) \theta_{ss} \tag{8}$$

(note that $(\theta_\tau - u)(\cos \theta)_s = (x_\tau + u^2/2)_s \theta_s$ holds due to (6b)). From Eqs. (7) and (8), we see

$$\{(\theta_{\tau} - u) \,\theta_{ss} - (\theta_{\tau s} - \sin \theta) \,\theta_{s}\} \cos \theta = 0.$$

If $\cos \theta \neq 0$ and $\theta_s \neq 0$ hold almost everywhere, we obtain

$$\left(\frac{\theta_{\tau} - u}{\theta_{s}}\right)_{s} = \frac{(\theta_{\tau} - u)\theta_{ss} - (\theta_{\tau s} - \sin\theta)\theta_{s}}{\theta_{s}^{2}} = 0.$$

If, furthermore, $\theta_{\tau}(\tau, 0) = u(\tau, 0)$ and $\theta_{s}(\tau, 0) \neq 0$ holds, we obtain

$$\frac{\theta_{\tau}(\tau,s)-u(\tau,s)}{\theta_{s}(\tau,s)}=\frac{\theta_{\tau}(\tau,0)-u(\tau,0)}{\theta_{s}(\tau,0)}=0,$$

which implies $\theta_{\tau} - u = 0$. It in turn implies

$$x_{\rm r} + \frac{u^2}{2} = 0 \tag{9}$$

from (7). Finally, by (8), we conclude $\theta_{\tau s} - \sin \theta = 0$, which is the desired sine-Gordon equation (2). Below, we consider the equivalence of the SP and the SG equations more precisely.

Before that, at this point let us show the overall picture of our strategy in Fig. 2. By "physical domain" we mean the SP equation on u(t,x) or $(x(\tau,s),u(\tau,s))$. As seen above, the SP equation is transformed to the SG equation on $\theta(\tau,s)$, which is called "computational domain". Our main strategy is to solve the SG equation (instead of the SP equation), and transform the solution back to the physical space. Note that we denote the length of the physical and computational domains by $L(\tau)$ and $S(\tau)$, stating the possibility of their dependence on time τ . The reason for this is because since we regard the variable s as the arc-length of the solution, $S(\tau)$ can vary in time in general (i.e., in general PDEs) if we fix L; similarly, $L(\tau)$ is allowed to depend on time if we fix S. It should be mathematically proved that they remain constants in the case of the SP and the SG equations.

Remark 2. Let us briefly comment on the difference between the standard moving mesh method and the approach here. In the standard method, after obtaining the parametrized PDE, one would furnish it with what we call "a moving mesh PDE (MMPDE)", which controls the grids. An advantage of this approach is that we can simply fix L and S as constants. Instead, there arises a difficulty that it is hard to find a counterpart of the implicit constraint $\int_0^L u(t,x)dx = 0$ in (5). In contrast, in the approach here, the constraint can be replicated as we will see later, but a careful discussion is necessary to guarantee that $L(\tau)$ and $S(\tau)$ stay fixed. In this sense, there is a trade-off between the two approaches.

Also note that, in view of Proposition 3, our method can be regarded as a special case of moving mesh methods whose moving mesh PDE is $x_{\tau} = -u^2/2$, which implies the mesh is distributed uniformly with respect to arc-length. However, unlike general moving mesh methods, we conducted further transformation with respect to θ and combine the system of PDEs (the SP equation and MMPDE) into a single PDE (the SG equation).

The discussion above has been already roughly done in the literature, but here we emphasize that the above reveals necessary constraint on the base point (see also Remark 4). Still, we should note that the deformations in the discussion above are not always mathematically rigorously equivalent, and we have to be careful exactly in which sense the solution of one equation solves the other. It seems this point as well has not been explicitly discussed in the literature.

We first show that any solution of the SG equation (2) solves the SP equation if the hodograph transformation satisfies the additional constraint

$$x_{\tau}(\tau,0) = -\frac{(\theta_{\tau}(\tau,0))^2}{2}, \qquad u(\tau,0) = \theta_{\tau}(\tau,0). \tag{10}$$

Note that here we leave the boundary condition open, and by "solution" we mean any functions that satisfy the equation on the specified interval.

Proposition 2. Let θ be a solution of the SG equation (2) on $s \in [0, S(\tau)]$, and (x, u) be a curve obtained via the hodograph transformation (6a) from $(x(\tau, 0), u(\tau, 0))$ satisfying (10). Then, (x, u) is a solution of the parametrized form (5) of the SP equation on $x \in [0, L(\tau)]$.

Proof. From the condition (10), we see

$$x_{\tau}(\tau, s) = x_{\tau}(\tau, 0) + \int_{0}^{s} (\cos \theta(\tau, \sigma))_{\tau} d\sigma = x_{\tau}(\tau, 0) - \int_{0}^{s} \sin \theta(\tau, \sigma)\theta_{\tau}(\tau, \sigma)d\sigma$$

$$= x_{\tau}(\tau, 0) - \int_{0}^{s} \theta_{\tau s}(\tau, \sigma)\theta_{\tau}(\tau, \sigma)d\sigma = x_{\tau}(\tau, 0) - \left[\frac{(\theta_{\tau}(\tau, \sigma))^{2}}{2}\right]_{0}^{s}$$

$$= -\frac{(\theta_{\tau}(\tau, s))^{2}}{2},$$

$$u(\tau, s) = u(\tau, 0) + \int_{0}^{s} \theta_{\tau s}(\tau, \sigma)d\sigma = u(\tau, 0) + [\theta_{\tau}(\tau, \sigma)]_{0}^{s} = \theta_{\tau}(\tau, s),$$
(11)

and therefore we obtain (9). This and (11) imply the relation (7) holds. Hence, (x, u) is a solution of (5). \Box

Furthermore, we can prove the converse under the assumption $x_s \neq 0$, i.e., as far as the solution is single-valued. This is related to the danger of using the parametrized form (5) when $x_s = 0$ can happen; this corresponds to the "mesh entanglement" issue in the context of the standard moving mesh method [32].

Proposition 3. Let u, x be a solution of the parametrized SP equation (5) on $x \in [0, L(\tau)]$ satisfying the condition (9). We assume $x_s(\tau, s) \neq 0$ holds for any $\tau \in \mathbb{R}_+$ and $s \in \mathbb{R}$. Then, the parameter s represents arc-length, i.e., the hodograph transformation (6a) and (6b) make sense and θ is uniquely determined. Furthermore, θ is a solution of the SG equation (2) on $s \in [0, S(\tau)]$.

Proof. Under the assumption $x_s \neq 0$, by substituting (9) and $x_{\tau s} = -uu_s$ (differentiation of (9) with respect to s) into (5), we see $u_{\tau s} = ux_s$. Thus, we obtain

$$\frac{\partial}{\partial \tau} (x_s^2 + u_s^2) = 2 (x_s x_{s\tau} + u_s u_{s\tau}) = 2 (x_s (-u u_s) + u_s (u x_s)) = 0.$$

Hence, the parameter s represents arc-length and the former part of the proposition holds true. Moreover, since the solution of (5) satisfies (8) and we assume $x_{\tau} + u^2/2 = 0$, we see $(\theta_{\tau s} - \sin \theta) \cos \theta = 0$. Finally, this equality and the assumption $x_s = \cos \theta \neq 0$ implies that $\theta_{\tau s} = \sin \theta$ holds. \Box

The discussion above (Propositions 2 and 3) rigorously justifies our strategy: we compute the numerical solution of the SG equation, and then we transform the solution by some discrete counterpart of the hodograph transformation (6a).

2.3. The fixed physical and computational domains

Next we prove that the lengths of the physical and computational domains are kept constant when the boundary condition is appropriate.

From Proposition 1, it is easy to see that $S(\tau) = S(u(\tau))$ does not depend on time under typical boundary conditions (including the periodic case) if $L(\tau)$ is fixed.

Its converse requires more careful discussion. To this end, it is essential to recall the fact that the SG equation (2) can be written in the variational form

$$\frac{\partial^2}{\partial \tau \partial s} \theta = \frac{\delta \mathcal{H}}{\delta \theta}, \qquad \mathcal{H}(\theta) = -\int_0^S \cos \theta(\tau, s) ds. \tag{12}$$

The value of the functional \mathcal{H} is kept invariant under certain boundary conditions.

Proposition 4. Under a boundary condition satisfying

$$\left[\frac{1}{2}\left(\theta_{\tau}(\tau,s)\right)^{2}\right]_{s}^{s}=0,\tag{13}$$

the solution of the variational form (12) satisfies $(d/d\tau)\mathcal{H}(\theta(\tau)) = 0$ for any $\tau \in \mathbb{R}_+$.

Proof. It can be shown by using (12) as follows:

$$\frac{\mathrm{d}}{\mathrm{d}\tau}\mathcal{H}(\theta) = \int_0^S \frac{\delta\mathcal{H}}{\delta\theta}\theta_{\tau}\mathrm{d}s = \int_0^S \theta_{\tau s}\theta_{\tau}\mathrm{d}s = \left[\frac{1}{2}\left(\theta_{\tau}(\tau,s)\right)^2\right]_0^S = 0. \quad \Box$$

The following lemma shows that the "window size in the physical domain", i.e., the value of $L(\tau)$, is given by the functional $\mathcal{H}(\theta)$.

Lemma 5. Suppose that $x, u : \mathbb{R}_+ \times [0, S] \to \mathbb{R}$ are obtained from $\theta : \mathbb{R}_+ \times [0, S] \to \mathbb{R}$ by (6a). Then, the relation $\mathcal{L}(x(\tau), u(\tau)) = -\mathcal{H}(\theta(\tau))$ holds for any $\tau \in \mathbb{R}_+$, where the functional $\mathcal{L} : C[0, S] \times C[0, S] \to \mathbb{R}$ is defined as $\mathcal{L}(f, g) := f(S) - f(0)$ for $f, g \in C[0, S]$.

Proof. Due to the hodograph transformation (6a), we see

$$\mathcal{L}\left(x(\tau),u(\tau)\right)=x(\tau,S)-x(\tau,0)=\int_{0}^{S}\cos\theta(\tau,s)\mathrm{d}s=-\mathcal{H}(\theta(\tau)),\quad\Box$$

which proves the lemma.

Thanks to Lemma 5 and Proposition 4, the window size remains constant as far as the boundary condition is appropriate.

Proposition 6. Let $\theta: \mathbb{R}_+ \times [0, S] \to \mathbb{R}$ be the solution of the SG equation (2) satisfying the condition (13). If $x, u: \mathbb{R}_+ \times [0, S] \to \mathbb{R}$ is obtained from θ by (6a), then $(d/d\tau)\mathcal{L}(x(\tau), u(\tau)) = 0$ holds for any $\tau \in \mathbb{R}_+$.

2.4. Treatment of the periodic boundary condition

So far we have left the boundary condition open. Now let us consider the particular case, the periodic boundary condition, to complete our framework in the continuous case.

The periodic boundary condition u(t, x + L) = u(t, x) ($\forall t \in \mathbb{R}_+$, $\forall x \in \mathbb{R}$) for the original form of the SP equation (1) corresponds to the boundary conditions

$$x(\tau, s+S) = x(\tau, s) + L, \quad u(\tau, s+S) = u(\tau, s) \qquad (\forall \tau \in \mathbb{R}_+, \ \forall s \in \mathbb{R}), \tag{14}$$

for the parametrized form (5). The following proposition provides the transformation of this to the world of θ . Recall that, thanks to Proposition 2, the solution curve obtained from that of the SG equation is a solution of the (parametrized) SP equation. Hence, the following proposition tells us the correspondence between the SP equation on the periodic domain and the SG equation on the (almost) periodic domain.

Proposition 7. Let $\theta(\tau, s)$ be the solution of the sine-Gordon equation (2) under the boundary condition

$$\theta(\tau, s+S) = \theta(\tau, s) + 2n\pi \qquad (\forall s \in [0, S])$$
(15)

for some $n \in \mathbb{Z}$. If $(x(\tau, s), u(\tau, s))$ is the curve obtained from $\theta(\tau, s)$ via the hodograph transformation (6a) with $(x(\tau, 0), u(\tau, 0))$ satisfying (10), then the periodic boundary condition (14) holds.

Proof. From (15) and the definition of the hodograph transformation (6a), we obtain

$$\begin{bmatrix} x(\tau,s+S) \\ u(\tau,s+S) \end{bmatrix} - \begin{bmatrix} x(\tau,s) \\ u(\tau,s) \end{bmatrix} = \int_{s}^{s+S} \begin{bmatrix} \cos\theta(\tau,\sigma) \\ \sin\theta(\tau,\sigma) \end{bmatrix} d\sigma = \int_{0}^{S} \begin{bmatrix} \cos\theta(\tau,\sigma) \\ \sin\theta(\tau,\sigma) \end{bmatrix} d\sigma.$$

Hence, the boundary condition (14) is equivalent to the equation

$$\int_0^S \begin{bmatrix} \cos \theta(\tau, \sigma) \\ \sin \theta(\tau, \sigma) \end{bmatrix} d\sigma = \begin{bmatrix} L \\ 0 \end{bmatrix}.$$

The equality above can be verified by the simple calculation:

$$\int_0^S \cos \theta(\tau, \sigma) d\sigma = -\mathcal{H}(\theta(\tau)) = -\mathcal{H}(\theta(0)) = x(0, S) - x(0, 0) = L,$$
(16)

$$\int_0^S \sin \theta(\tau, \sigma) d\sigma = \int_0^S \theta_{\tau s}(t, \sigma) d\sigma = [\theta_{\tau}(\tau, \sigma)]_0^S = 0.$$
 (17)

Here, we use Proposition 4 and the boundary condition (15). \Box

Note that, the integer n is determined by the initial condition $\theta(0, s)$, and remains constant along time evolution thanks to the continuity of the solution. Note also that the condition (15) implies (13), and thus Proposition 6 holds; i.e., L does not depend on time. This is extremely important, since "periodic solution" would lose its meaning if $L(\tau)$ were changing.

2.5. Recovery of the implicit constraint

Since L successfully becomes a constant, it makes sense to consider the implicit constraint $\int_0^L u(t,x) dx = 0$. This is successfully kept by the solution u generated from the solution θ of the SG equation. Let $x(\tau,s)$, $u(\tau,s)$ be the pair obtained from the solution $\theta(\tau,s)$ of the SG equation under the boundary condition (15). Then we have

$$\int_{0}^{L} u(t, x) dx = \int_{0}^{S} u(\tau, s) x_{s}(\tau, s) ds$$

$$= \int_{0}^{S} \left(u(\tau, 0) + \int_{0}^{s} \sin \theta(\tau, \sigma) d\sigma \right) \cos \theta(\tau, s) ds$$

$$= \int_{0}^{S} \left(u(\tau, 0) + \int_{0}^{s} \theta_{\tau s}(\tau, \sigma) d\sigma \right) \cos \theta(\tau, s) ds$$

$$= \int_{0}^{S} \left(u(\tau, 0) + \theta_{\tau}(\tau, s) - \theta_{\tau}(\tau, 0) \right) \cos \theta(\tau, s) ds$$

$$= \left(u(\tau, 0) - \theta_{\tau}(\tau, 0) \right) \int_{0}^{S} \cos \theta(\tau, s) ds + \frac{d}{d\tau} \int_{0}^{S} \sin \theta(\tau, s) ds,$$

where the first and second terms vanish due to (10) and (17), respectively.

3. Proposed scheme for the SP equation

We here present the proposed scheme. First we show the outline in Section 3.1, and its detail in the subsequent subsections.

3.1. Outline

We give the outline of the proposed scheme for the SP equation. Let us introduce the discrete variables $\theta_k^{(m)}$ approximating $\theta(m\Delta\tau, k\Delta s)$ ($k \in \mathbb{Z}$; m = 0, 1, ..., M), where $\Delta\tau$ and Δs are the mesh sizes. Here, in view of Proposition 7, we impose the discrete boundary condition

$$\theta_{k+K}^{(m)} = \theta_k^{(m)} + 2n\pi \qquad (k \in \mathbb{Z}; \ m = 0, 1, \dots, M+1),$$
 (18)

where $n \in \mathbb{Z}$ is a fixed constant determined by the initial condition. We also introduce the vector notation $\theta^{(m)} :=$ $(\theta_1^{(m)},\dots,\theta_K^{(m)})^{\top}.$ The outline of the proposed scheme is defined as follows.

Proposed scheme for the SP equation

Step 0: Prepare the initial condition $\theta_k^{(0)}$ ($k \in \mathbb{Z}$) of the SG equation, and set $n := (\theta_k^{(0)} - \theta_0^{(0)})/(2\pi)$ (Section 3.2).

Step 1: Compute $\theta_k^{(m)}$ (k = 1, ..., K; m = 1, ..., M + 1) by using (20) under the boundary condition (18) (Section 3.3).

Step 2: Compute $x_k^{(m)}, u_k^{(m)}$ (k = 0, ..., K - 1; m = 0, 1, ..., M), which are approximate solutions for $x(\tau, s), u(\tau s)$, by using (23) with $(x_0^{(m)}, u_0^{(m)})$ defined by (25) (Section 3.4).

3.2. Step 0: Preparation of the initial data $\theta^{(0)}$

We can think of two different cases depending on how the initial data for the SP equation is given.

The first possibility is the case that the initial condition is directly given in the parametrized form (x(0, s), u(0, s)); all multi-valued solutions, and some particular solutions of interest such as (3), are given in this way. In this case, we can prepare the initial data $\theta^{(0)}$ directly in the computational domain. We first choose an appropriate S, the length of the computational domain (possibly depending on the period of the solution). Then $\theta^{(0)}$ can be computed by either of the following two ways. If the initial condition is given analytically as functions, the function $\theta(0,s)$ can be found easily by (6b) as $\theta(0, s) = \arctan(u_s/x_s)$. We can then evaluate the function on the grid points $s = k\Delta s$ (k = 1, ..., K). Cares are necessary to the argument range and on some points where $x_s = 0$, but this is straightforward by making the resulting function continuous. If, on the other hand, (x(0, s), u(0, s)) is given only numerically, for example, only as a program subroutine, and accordingly known only on the grid points, we can replace the derivatives u_s and x_s above by some finite differences; for example, we can set (again with some care)

$$\theta_k^{(0)} = \arctan\left(\frac{u_k^{(0)} - u_{k-1}^{(0)}}{x_k^{(0)} - x_{k-1}^{(0)}}\right), \qquad (k = 1, \dots, K).$$
(19)

The second possibility is that the initial condition is given for the original SP equation (1) as $u_0(x)$, which is more natural setting as an initial value problem for (1), although it intrinsically allows only single-valued solutions. In this case, a possible strategy to prepare $\theta^{(0)}$ is as follows. We first find the total arc-length $\mathcal{S}(u_0)$ by an accurate numerical integration (recall Section 2.1), and set $S = S(u_0)$. The remaining task is to find $x^{(0)}$ and $u^{(0)}$ on the grid points $s = k\Delta s$, which reduces the discussion to the first case above. An obvious way to do this is to numerically solve for each k (k = 1, ..., K)

$$\int_0^x \sqrt{1 + (u_{0,\xi}(\xi))^2} d\xi = k\Delta s$$

by, for example, the Newton iteration, to obtain $x_k^{(0)}$ (in above, $u_{0,\xi}$ means $\partial u_0/\partial \xi$). There, we can use the exact derivative $u_{0,\xi}$ of the initial condition u_0 when available, while we employ some finite differences otherwise. Then we can compute $\theta^{(0)}$ by, for example, $\theta_k^{(0)} := \arctan(u_x(0,x_k^{(0)}))$ (it is also possible to set $u_k^{(0)} = u_0(x_k^{(0)})$, but this is not necessary; it will be computed back from θ). Another possible way is to employ a method to realize the "equidistribution principle" in the standard moving mesh method [31, Chap. 2]. In the setting of this paper, the distance is measured by the arc-length (i.e., in terms of the mesh density function, $\rho(x) = \sqrt{1 + u_x^2}$, in the notation of [31, Section 2.4.3]). Note that, however, in the standard moving mesh method, often a rough realization of equidistribution is sufficient for practical purposes, and the resulting grid may not be strictly equidistributing, depending on the algorithm. This can cause a severe accuracy degeneration in preparing $\theta^{(0)}$ in the present context, since we demand s to be the strict arc-length. In this sense, we should employ an accurate equidistribution method, or alternatively, a combination of a rough method and the Newton iteration refinement.

3.3. Step 1: Solving the SG equation by a conservative method

As seen in Section 2.3, the preservation of the functional \mathcal{H} in the SG equation is indispensable for keeping the physical window size constant. The discrete variational derivative method [44] (DVDM; see also Furihata–Matsuo [45]) gives a way to construct such a special scheme. Although the original DVDM did not cover the SG equation (12), where an additional differential operator with respect to the spatial variable s is included in the left hand side, later it has been extended to accommodate such cases [46,47]. Furthermore, recently, a scheme with better stability was proposed in [48]. Below we show a scheme for the SG equation employing their technique.

Let us first introduce the spatial forward difference and average operators

$$\delta_s^+ \theta_k^{(m)} = \frac{\theta_{k+1}^{(m)} - \theta_k^{(m)}}{\Delta s}, \qquad \qquad \mu_s^+ \theta_k^{(m)} = \frac{\theta_{k+1}^{(m)} + \theta_k^{(m)}}{2},$$

and the spatial backward difference and average operators

$$\delta_s^- \theta_k^{(m)} = \frac{\theta_k^{(m)} - \theta_{k-1}^{(m)}}{\Delta s}, \qquad \qquad \mu_s^- \theta_k^{(m)} = \frac{\theta_k^{(m)} + \theta_{k-1}^{(m)}}{2}.$$

Here, the subscript s denotes the spatial operator, and the temporal counterparts δ_{τ}^+ , μ_{τ}^+ , δ_{τ}^- , μ_{τ}^- are similarly defined. First of all, we define a discrete version $\mathcal{H}_{\rm d}$ of the functional \mathcal{H} as

$$\mathcal{H}_{d}(\theta^{(m)}) = -\sum_{k=1}^{K} \cos \theta_{k}^{(m)} \Delta s.$$

Then, the discrete variational derivative $\delta \mathcal{H}_d / \delta(\theta^{(m+1)}, \theta^{(m)})_k$ of \mathcal{H}_d is defined as a function satisfying the relation

$$\delta_{\tau}^{+}\mathcal{H}_{d}\left(\boldsymbol{\theta}^{(m)}\right)=\sum_{k=1}^{K}\frac{\delta\mathcal{H}_{d}}{\delta(\boldsymbol{\theta}^{(m+1)},\boldsymbol{\theta}^{(m)})_{k}}\delta_{\tau}^{+}\boldsymbol{\theta}_{k}^{(m)}\Delta\boldsymbol{s},$$

and in this case, it can be derived as

$$\frac{\delta \mathcal{H}_{d}}{\delta(\theta^{(m+1)}, \theta^{(m)})_{k}} = -\frac{\cos \theta_{k}^{(m+1)} - \cos \theta_{k}^{(m)}}{\theta_{k}^{(m+1)} - \theta_{k}^{(m)}} \quad (k = 1, 2, \dots, K).$$

By using this, we define an average-difference scheme: for m = 0, 1, 2, ..., and k = 1, ..., K,

$$\delta_s^+ \delta_\tau^+ \theta_k^{(m)} = \mu_s^+ \frac{\delta \mathcal{H}_d}{\delta(\theta^{(m+1)}, \theta^{(m)})_k}.$$
 (20)

Proposition 8 (cf. [48, Theorem 1]). Let $\theta_k^{(m)}$ be the solution of the discrete variational derivative method (20) with a boundary condition satisfying

$$\left[\left(\delta_{\tau}^{+}\theta_{k}^{(m)}-\frac{\Delta s}{2}\frac{\delta\mathcal{H}_{d}}{\delta(\theta^{(m+1)},\theta^{(m)})_{k}}\right)^{2}\right]_{1}^{K+1}=0.$$

Then, it holds that $\mathcal{H}_d(\theta^{(m+1)}) = \mathcal{H}_d(\theta^{(m)})$ for any m = 0, ..., M.

Since the proof of Proposition 8 is rather complicated and the full proof has already appeared in [48], we omit it here.

Remark 3. In discretizing (12), one may be tempted to employ some standard skew-symmetric difference operators such as the central difference operator, the compact difference operator (see, e.g., [49]), and the Fourier-spectral difference operator (see, e.g., [50]), since the skewness is basically the source of the conservation. For example, by using the central difference operator $\delta_s^{(1)}: u_k^{(m)} \mapsto (u_{k+1}^{(m)} - u_{k-1}^{(m)})/2\Delta s$, which is the simplest skew-symmetric difference operator, we can also construct a conservative method

$$\delta_s^{(1)} \delta_\tau^+ \theta_k^{(m)} = \frac{\delta \mathcal{H}_d}{\delta(\theta^{(m+1)}, \theta^{(m)})_\nu}.$$
 (21)

Although the numerical method certainly conserves the value of \mathcal{H}_d , it suffers from undesirable spatial oscillations (see, [48]).

3.4. Step 2: Obtaining the solution by a discrete hodograph transformation

The remaining task is to give a formula to transform $\theta^{(m)}$ back to $x^{(m)}$ and $u^{(m)}$. If we employ the natural discretization

$$\begin{bmatrix} x_k^{(m)} \\ u_h^{(m)} \end{bmatrix} = \begin{bmatrix} x_0^{(m)} \\ u_0^{(m)} \end{bmatrix} + \sum_{i=1}^k \begin{bmatrix} \cos \theta_i^{(m)} \\ \sin \theta_i^{(m)} \end{bmatrix} \Delta s, \tag{22}$$

of the hodograph transformation (6a), the periodic boundary condition is not satisfied in the physical domain; in fact, $u_K^{(m)} - u_0^{(m)} = \sum_{k=1}^K \sin\theta_k^{(m)} \Delta s$ does not coincide with 0. The reason lies in the fact that the discrete counterpart of (17) does not hold in general, due to the difference between the right-hand side of the discrete sine-Gordon equation (20) and the $\sin\theta_i^{(m)}$ in (22). For the case of the periodic domain, this problem is serious, since it means $u_K^{(m)} \neq u_0^{(m)}$, and thus there appears a gap in u around the base point $x_0^{(m)}$.

We can overcome this difficulty by carefully redefining the discrete hodograph transformation as

$$\begin{bmatrix} x_k^{(m)} \\ u_k^{(m)} \end{bmatrix} = \begin{bmatrix} x_0^{(m)} \\ u_0^{(m)} \end{bmatrix} + \sum_{i=1}^k \begin{bmatrix} \cos \theta_i^{(m)} \\ \mu_s^- \frac{\delta \mathcal{H}_d}{\delta \left(\theta^{(m+1)}, \theta^{(m)} \right)_i} \end{bmatrix} \Delta s, \tag{23a}$$

$$\begin{bmatrix} \delta_s^- x_k^{(m)} \\ \delta_s^- u_k^{(m)} \end{bmatrix} = \begin{bmatrix} \cos \theta_k^{(m)} \\ \theta_s^- \frac{\delta \mathcal{H}_d}{\delta \left(\theta^{(m+1)}, \theta^{(m)} \right)_k} \end{bmatrix}. \tag{23b}$$

To prove it works fine, we start by showing the following lemma, which corresponds to Lemma 5.

Lemma 9. Suppose that $(x_k^{(m)}, u_k^{(m)})$ is obtained from $\theta_k^{(m)}$ by using (23a). Then, the relation $\mathcal{L}\left(x^{(m)}, u^{(m)}\right) = -\mathcal{H}\left(\theta^{(m)}\right)$ holds for any $m = 0, 1, \ldots, M$, where the functional \mathcal{L} is defined as $\mathcal{L}(x^{(m)}, u^{(m)}) = x_K^{(m)} - x_0^{(m)}$.

Proof. It can be shown by the simple calculation:

$$\mathcal{L}(x^{(m)}, u^{(m)}) = x_K^{(m)} - x_0^{(m)} = \sum_{i=1}^K \cos \theta_i^{(m)} \Delta s = -\mathcal{H}_d(\theta^{(m)}). \quad \Box$$

The value of the functional $\mathcal{L}(x^{(m)}, u^{(m)})$ represents the window size in the physical space. Thanks to Lemma 9 and the consistent definition (23a), we can follow the line of the discussion in the proof of Proposition 7.

Theorem 10. Let $\theta_k^{(m)}$ $(k \in \mathbb{Z}; m = 0, \dots, M+1)$ be the solution of the discrete sine-Gordon equation (20) under the boundary condition (18) for some $n \in \mathbb{Z}$. If $(x_k^{(m)}, u_k^{(m)})$ is the curve obtained from $\theta_k^{(m)}$ via the discrete hodograph transformation (23a) with some $(x_0^{(m)}, u_0^{(m)})$, then $(x_k^{(m)}, u_k^{(m)})$ satisfies the boundary condition

$$x_{k+K}^{(m)} = x_k^{(m)} + L_d, \quad u_{k+K}^{(m)} = u_k^{(m)} \qquad (k \in \mathbb{Z}; \ m = 0, \dots, M+1),$$
 (24)

where the constant L_d is determined by the initial condition $L_d := -\mathcal{H}_d(\theta^{(0)})$, and is an approximation of the original physical domain size L.

Proof. From the boundary condition (18) and the definition (23a) of the discrete hodograph transformation, we obtain

$$\begin{bmatrix} x_{k+K}^{(m)} \\ u_{k+K}^{(m)} \end{bmatrix} - \begin{bmatrix} x_k^{(m)} \\ u_k^{(m)} \end{bmatrix} = \sum_{i=k+1}^{k+K} \begin{bmatrix} \cos\theta_i^{(m)} \\ \mu_s^- \frac{\delta\mathcal{H}_d}{\delta\left(\theta^{(m+1)}, \theta^{(m)}\right)_i} \end{bmatrix} \Delta s = \sum_{i=1}^K \begin{bmatrix} \cos\theta_i^{(m)} \\ \mu_s^- \frac{\delta\mathcal{H}_d}{\delta\left(\theta^{(m+1)}, \theta^{(m)}\right)_i} \end{bmatrix} \Delta s.$$

Hence, the boundary condition (24) is equivalent to the equation

$$\sum_{i=1}^{K} \begin{bmatrix} \cos \theta_{i}^{(m)} \\ \mu_{s}^{-} \frac{\delta \mathcal{H}_{d}}{\delta \left(\theta^{(m+1)}, \theta^{(m)} \right)_{i}} \end{bmatrix} \Delta s = \begin{bmatrix} L_{d} \\ 0 \end{bmatrix}.$$

The equality above can be verified by following the line of the discussion in the proof of Proposition 7 as follows:

$$\sum_{i=1}^{K} \cos \theta_{i}^{(m)} \Delta s = -\mathcal{H}_{d} \left(\theta^{(m)} \right) = -\mathcal{H}_{d} \left(\theta^{(0)} \right),$$

$$\sum_{i=1}^K \mu_s^- \frac{\delta \mathcal{H}_d}{\delta \left(\theta^{(m+1)}, \theta^{(m)}\right)_i} \Delta s = \sum_{i=0}^{K-1} \mu_s^+ \frac{\delta \mathcal{H}_d}{\delta \left(\theta^{(m+1)}, \theta^{(m)}\right)_i} \Delta s = \sum_{i=0}^{K-1} \delta_s^+ \delta_\tau^+ \theta_i^{(m)} \Delta s = 0.$$

Here, we use Proposition 8 and the boundary condition (18). Note that the first identity exactly corresponds to (16). The second is formally different from (17), although the correspondence holds in the continuous limit. \Box

Our final task is to give a method to compute $(x_0^{(m)}, u_0^{(m)})$. We can do this by defining a discrete counterpart of the condition (10), which describes the time evolution of the base point. Fortunately, Theorem 10 reveals that regardless of this choice the discrete boundary condition is guaranteed. Let us here choose a discrete counterpart as follows:

$$x_0^{(m+1)} = x_0^{(m)} - \frac{\Delta \tau}{2} \left(u_0^{(m)} \right)^2, \tag{25a}$$

$$u_0^{(m)} = \delta_{\tau}^{+} \theta_0^{(m)} - \frac{\sum_{k=1}^{K} \left(\delta_{\tau}^{+} \theta_k^{(m)}\right) \cos \theta_k^{(m)} \Delta s}{\sum_{k=1}^{K} \cos \theta_k^{(m)} \Delta s}.$$
 (25b)

For (25b), one might think that a simpler definition $u_0^{(m)} = \delta_{\tau}^+ \theta_0^{(m)}$ would suffice, and (25b) is an unnecessary complication. But it is necessary to replicate the implicit constraint $\int_0^L u(t,x) dx = 0$ of the SP equation. Recall the discussion in Section 2.5; we here copy it in the discrete setting. For the numerical solution, $x_k^{(m)}$, $u_k^{(m)}$, we see that (with an abbreviation $a_k := \delta \mathcal{H}_d / \delta(\theta^{(m+1)}, \theta^{(m)})_k$)

$$\begin{split} \sum_{k=1}^{K} u_{k}^{(m)} \left(x_{k}^{(m)} - x_{k-1}^{(m)} \right) &= \sum_{k=1}^{K} \left(u_{0}^{(m)} + \sum_{i=1}^{k} \mu_{s}^{-} a_{i} \Delta s \right) \cos \theta_{k}^{(m)} \Delta s \\ &= \sum_{k=1}^{K} \left(u_{0}^{(m)} + \sum_{i=0}^{k-1} \mu_{s}^{+} a_{i} \Delta s \right) \cos \theta_{k}^{(m)} \Delta s \\ &= \sum_{k=1}^{K} \left(u_{0}^{(m)} + \sum_{i=0}^{k-1} \delta_{s}^{+} \delta_{\tau}^{+} \theta_{i}^{(m)} \Delta s \right) \cos \theta_{k}^{(m)} \Delta s \\ &= \sum_{k=1}^{K} \left(u_{0}^{(m)} + \delta_{\tau}^{+} \theta_{k}^{(m)} - \delta_{\tau}^{+} \theta_{0}^{(m)} \right) \cos \theta_{k}^{(m)} \Delta s \\ &= \left(u_{0}^{(m)} - \delta_{\tau}^{+} \theta_{0}^{(m)} \right) \sum_{k=1}^{K} \cos \theta_{k}^{(m)} \Delta s + \sum_{k=1}^{K} \cos \theta_{k}^{(m)} \delta_{\tau}^{+} \theta_{k}^{(m)} \Delta s. \end{split}$$

It successfully vanishes under (25b). This is the desired discrete constraint.

Note that (25a) (or its continuous counterpart (10)) implies that the base point moves along time. This might seem strange at first sight, but this is necessary; the whole framework becomes consistent only under this situation.

Remark 4. Let us here summarize the intrinsic difference between the \mathbb{R} and the periodic cases. The vanishing condition on \mathbb{R} can be approximated by setting a sufficiently large window [0, L], and by imposing Dirichlet boundary condition $u(t, 0) = u(t, L) = u_x(t, 0) = u_x(t, L) = 0$ (actually this is often employed in the integrable systems studies). The corresponding boundary condition for the SG equation is simply the Dirichlet boundary condition $\theta(\tau, 0) = \theta(\tau, S) = 0$ (or $= 2n\pi$ for loop solitons). This greatly simplifies the discussion carefully carried out in the present paper; the condition (10) is trivially satisfied with $x(\tau, 0) = 0$, $u(\tau, 0) = 0$ (i.e., in this case the base point does not move), and accordingly, we do not need (25). We also note that the assumption on the discrete boundary condition of the discrete conservation law (Proposition 8) holds, and the counterpart of Theorem 10 can be similarly proved. In this way, the results in this paper trivially apply also to the \mathbb{R} case.

Another note should go to the fact that, if we employ the simple discrete hodograph transformation (22) instead of (23a), we can prove the boundedness of the solution curve [51]. On the other hand, the discrete boundary condition corresponding to u(t, L) = 0 no longer exactly holds, i.e., the counterpart of Theorem 10 ceases to work.

4. Numerical examples

In order to compare with the proposed scheme, we here also introduce two schemes, a norm-preserving scheme and the multi-symplectic scheme [26]. They are structure-preserving methods and widely known to be much stabler than generic methods for tough problems, and they are expected to be the first choice for the short pulse equation. All the schemes are nonlinearly implicit, but through preliminary numerical tests we have an impression that explicit methods are not robust enough for long time integration of some solutions near or with singularity we consider here. In fact, even the nonlinearly implicit norm-preserving scheme, which is thus "energy stable" in the usual sense, exhibits instability. We solved nonlinear equations simply by 'fsolve' of MATLAB; in this paper we do not step into fast implementation of nonlinear solvers, and leave it to future works.

4.1. Structure-preserving schemes on fixed uniform mesh for comparison

First, we show a norm-preserving scheme for the SP equation on the fixed uniform mesh, which has already appeared in Introduction (Fig. 1). Here we skip some mathematical details, which are left to the Appendix.

On the fixed mesh, the symbol $\overline{u}_k^{(m)}$ denotes the approximation of $u(m\Delta t, k\Delta x)$ for $m=0,1,\ldots,M$ and $k\in\mathbb{Z}$, and we assume the periodic boundary condition $\overline{u}_{k+N}^{(m)}=\overline{u}_k^{(m)}$ (N is a fixed integer satisfying $N\Delta x=L$). As a discrete counterpart of the norm \mathcal{I} , we define

$$\overline{\mathcal{I}}_{\mathsf{d}}(\overline{u}_{k}^{(m)}) := \frac{1}{2} \sum_{k=1}^{N} \left(\overline{u}_{k}^{(m)} \right)^{2} \Delta x.$$

Since the norm $\overline{\mathcal{I}}_d$ is a quadratic invariant, we can easily construct the norm-preserving scheme as

$$\delta_t^+ \overline{u}_k^{(m)} = \delta_{FD}^{-1} \mu_t^+ \overline{u}_k^{(m)} + \frac{1}{6} \delta_x^- \left(\left(\mu_x^+ \left(\mu_t^+ \overline{u}_k^{(m)} \right)^2 \right) \mu_x^+ \mu_t^+ \overline{u}_k^{(m)} \right), \tag{26}$$

where the discrete counterpart δ_{FD}^{-1} of the generalized inverse ∂_x^{-1} is defined as

$$\delta_{\mathrm{FD}}^{-1}\overline{u}_{k}^{(m)} := \widetilde{\delta}_{\mathrm{FD}}^{-1}\overline{u}_{k}^{(m)} - \frac{1}{N\Delta x} \sum_{\ell=1}^{N} \widetilde{\delta}_{\mathrm{FD}}^{-1}\overline{u}_{\ell}^{(m)} \Delta x,$$

$$\tilde{\delta}_{\text{FD}}^{-1} \overline{u}_{k}^{(m)} := \begin{cases} \overline{u}_{N}^{(m)} + \overline{u}_{1}^{(m)} \Delta x & (k = 1), \\ 2 & 2 \\ \left(\frac{1}{2} \overline{u}_{N}^{(m)} + \sum_{\ell=1}^{k-1} \overline{u}_{\ell}^{(m)} \Delta x + \frac{1}{2} \overline{u}_{k}^{(m)}\right) \Delta x & (\text{otherwise}) \end{cases}$$

(it is devised by Yaguchi-Matsuo-Sugihara [47] for the Ostrovsky equation).

The scheme (26) is mathematically equivalent to

$$\delta_x^+ \delta_t^+ \overline{u}_k^{(m)} = \mu_x^+ \mu_t^+ \overline{u}_k^{(m)} + \frac{1}{6} \delta_x^{(2)} \left(\left(\mu_x^+ \left(\mu_t^+ \overline{u}_k^{(m)} \right)^2 \right) \mu_x^+ \mu_t^+ \overline{u}_k^{(m)} \right), \tag{27}$$

which is more convenient to implement since it does not include non-local operators (see discussions in [43]), and will be used in the following numerical experiments.

The scheme (26) (and accordingly (27)) enjoys the desired preservation.

Proposition 11. Let $\overline{u}_k^{(m)}$ be the numerical solution of the scheme (26) under the periodic boundary condition and initial condition satisfying $\sum_k \overline{u}_k^{(0)} = 0$. Then, $\overline{\mathcal{I}}_d(\overline{u}^{(m+1)}) = \overline{\mathcal{I}}_d(\overline{u}^{(m)})$ holds.

Next we show the multi-symplectic scheme given in [26]. They found a multi-symplectic form of the SP equation, and applied the Preissman-box scheme [52] to it. By eliminating redundant variables in Pietrzyk–Kanattšikov's scheme, we find

$$\delta_x^+\delta_t^+ \left(\mu_x^+\right)^2 \overline{u}_k^{(m)} = \mu_t^+ \left(\mu_x^+\right)^3 \overline{u}_k^{(m)} + \frac{1}{6} \left(\delta_x^+\right)^2 \left(\mu_t^+ \mu_x^+ \overline{u}_k^{(m)}\right)^3.$$

By further rewriting $\overline{u}_k^{(m)} = \mu_x^+ \overline{u}_k^{(m)}$, the scheme above can be simplified into

$$\delta_{x}^{(1)}\delta_{t}^{+}\overline{u}_{k}^{(m)} = \mu_{t}^{+}\mu_{x}^{(2)}\overline{u}_{k}^{(m)} + \frac{1}{6}\delta_{x}^{(2)}\left(\mu_{t}^{+}\overline{u}_{k}^{(m)}\right)^{3},\tag{28}$$

where $\delta_x^{(2)}\overline{u}_k^{(m)} := (\overline{u}_{k+1}^{(m)} - 2\overline{u}_k^{(m)} + \overline{u}_k^{(m)})/(\Delta x)^2$ and $\mu_x^{(2)}\overline{u}_k^{(m)} := (\overline{u}_{k+1}^{(m)} + 2\overline{u}_k^{(m)} + \overline{u}_k^{(m)})/4$. It should be noted that the solutions of this numerical scheme almost preserve \mathcal{I} and \mathcal{E} [53]. For the general theory of multi-symplectic integrators, see Bridges–Reich [52].

4.2. Numerical examples for smooth pulse solution near and far from the criticality

First of all, we consider the pulse solution (3) with $\xi=0.3$, which is relatively far from the criticality, and thus still rather safe for standard integrators. Figs. 3–6 show the results of the norm-preserving scheme (27), the multi-symplectic scheme (28), and the proposed scheme. The parameters are taken to K=N=511, $\Delta t=0.01$, S=70, L=66.96. The initial data $\theta^{(0)}$ is prepared by the finite difference approximation (19), which seems fine judging from the results below. The initial data $\overline{u}^{(0)}$ on the uniform mesh, which is necessary in the standard methods (27) and (28), is prepared by numerically solving the nonlinear equation $x(0, k\Delta s) = k\Delta x$ whose left-hand side is the exact solution (3) (again, we simply employ 'fsolve' of MATLAB).

Figs. 3 and 4 show the snapshots at t=50 and t=100. Until t=50, all the schemes work more or less fine. It agrees with the insight obtained in [26], where in further safer regime $\xi=0.2$ the multi-symplectic scheme, a structure-preserving scheme, worked well and was advantageous over a standard pseudospectral method, which is not structure-preserving. At t=100, we find that the norm-preserving scheme and the proposed scheme keep working. We see, however, tiny numerical oscillations in the multi-symplectic scheme.

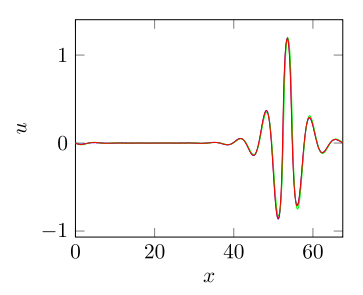


Fig. 3. Numerical solutions at t = 50 corresponding to the pulse solution (3) with $\xi = 0.30$ (N = 511, $\Delta t = 0.01$). Solid lines in red, green, and blue are numerical solutions of the proposed scheme, the standard norm-preserving scheme, and the multi-symplectic scheme respectively. (For interpretation of the references to color in this figure legend, the reader is referred to the web version of this article.)

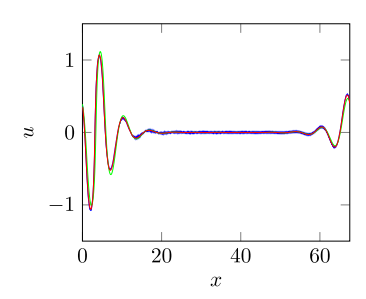


Fig. 4. Numerical solutions at t = 100 corresponding to the pulse solution (3) with $\xi = 0.30$ (N = 511, $\Delta t = 0.01$). Solid lines in red, green, and blue are numerical solutions of the proposed scheme, the standard norm-preserving scheme, and the multi-symplectic scheme respectively. (For interpretation of the references to color in this figure legend, the reader is referred to the web version of this article.)

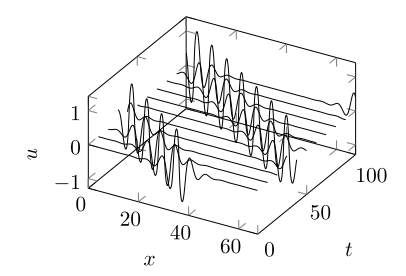


Fig. 5. The numerical solution of the proposed scheme under the initial condition (3) with $\xi = 0.30$ (K = 511, $\Delta t = 0.01$).

Fig. 6 shows that the preservation of the invariants is consistent with the construction of the schemes; "NP" means the norm-preserving scheme, "MS" the multi-symplectic scheme, and "SG" the proposed scheme. There, the discrete counterpart $\overline{\mathcal{E}}_d$ of the energy on the uniform mesh is defined as

$$\overline{\mathcal{E}}_{\mathrm{d}}(\overline{u}^{(m)}) := \sum_{k=1}^{N} \left(\frac{1}{24} \left(\overline{u}_{k}^{(m)} \right)^{4} - \frac{1}{2} \left(\delta_{\mathrm{FD}}^{-1} \overline{u}_{k}^{(m)} \right)^{2} \right),$$

and the discrete counterparts \mathcal{E}_d and \mathcal{I}_d of the energy \mathcal{E} and the norm \mathcal{I} on the moving mesh are defined as

$$\begin{split} \mathcal{E}_{\mathrm{d}}(x^{(m)}, u^{(m)}) &:= \sum_{k=1}^{K} \left(\frac{1}{24} \left(u_{k}^{(m)} \right)^{4} + \frac{1}{2} \left(\phi_{k}^{(m)} \right)^{2} \right) \left(x_{k}^{(m)} - x_{k-1}^{(m)} \right), \\ \mathcal{I}_{\mathrm{d}}(x^{(m)}, u^{(m)}) &:= \frac{1}{2} \sum_{k=1}^{K} \left(u_{k}^{(m)} \right)^{2} \left(x_{k}^{(m)} - x_{k-1}^{(m)} \right), \end{split}$$

where $\phi_k^{(m)} \approx \partial^{-1} u(m\Delta \tau, x(m\Delta \tau, k\Delta s))$ is defined as

$$\phi_k^{(m)} := \tilde{\phi}_k^{(m)} - \frac{1}{L} \sum_{\ell=1}^K \tilde{\phi}_\ell^{(m)} (x_\ell^{(m)} - x_{\ell-1}^{(m)}), \qquad \qquad \tilde{\phi}_k^{(m)} := \sum_{\ell=1}^k \mu_s^- u_\ell^{(m)} (x_\ell^{(m)} - x_{\ell-1}^{(m)}).$$

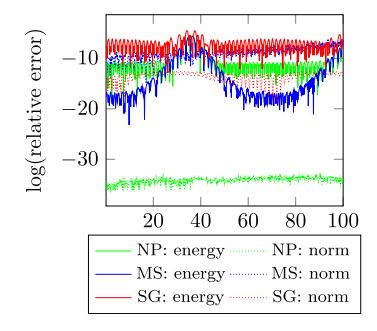


Fig. 6. The evolution of the logarithm of the relative errors of the norm \mathcal{I} and the energy \mathcal{E} for each numerical solutions. (For interpretation of the references to color in this figure legend, the reader is referred to the web version of this article.)

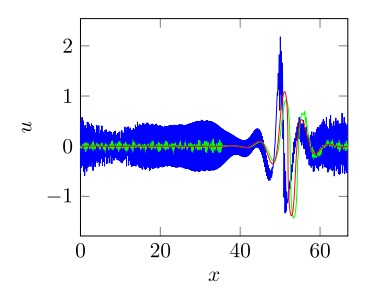


Fig. 7. Numerical solutions at t = 50 corresponding to the pulse solution (3) with $\xi = 0.38$ (N = 511, $\Delta t = 0.01$). Solid lines in red, green, and blue are numerical solutions of the proposed scheme, the standard norm-preserving scheme, and the multi-symplectic scheme respectively. (For interpretation of the references to color in this figure legend, the reader is referred to the web version of this article.)

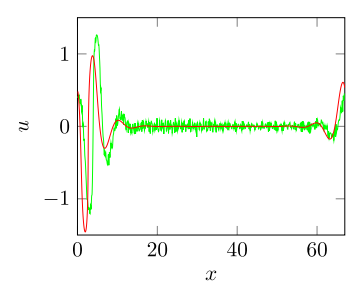


Fig. 8. Numerical solutions at t = 100 corresponding to the pulse solution (3) with $\xi = 0.38$ (N = 511, $\Delta t = 0.01$). Solid lines in red and green are numerical solutions of the proposed scheme and the standard norm-preserving scheme, respectively. (For interpretation of the references to color in this figure legend, the reader is referred to the web version of this article.)

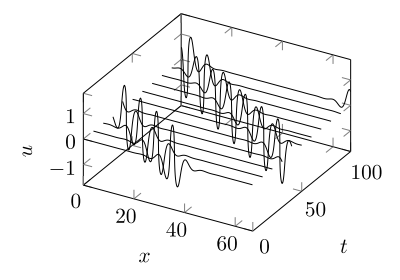


Fig. 9. The numerical solution of the proposed scheme under the initial condition (3) with $\xi = 0.38$ (K = 511, $\Delta t = 0.01$).

Now let us turn our attention to the severer case $\xi = 0.38$, for which results are shown in Figs. 7–11 (K = N = 511, $\Delta t = 0.01$, S = 70, L = 67.6). The multi-symplectic scheme cannot withstand anymore at all, and exhibits severe oscillations. In some tests the authors observe such visible oscillations persist even if we take a very fine mesh with N = 2047. We also find undesirable oscillations in the norm-preserving scheme as well; the scheme works for $\xi = 0.30$,

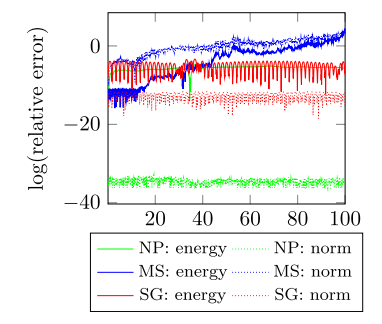


Fig. 10. The evolution of the logarithm of the relative errors of the norm \mathcal{I} and the energy \mathcal{E} for each numerical solutions. (For interpretation of the references to color in this figure legend, the reader is referred to the web version of this article.)

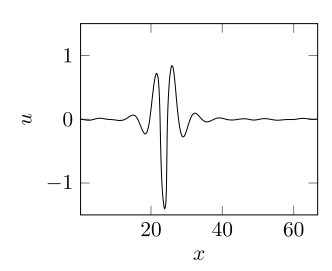


Fig. 11. The numerical solution of the proposed scheme corresponding to the pulse solution (3) with $\xi = 0.38$ (K = 127, $\Delta t = 0.1$) at t = 1000.

but it does not for the severer setting. The subcritical solution with $\xi=0.38$ has a very steep region where the argument is quite close to $\pi/2$; in various numerical experiments we observe that the norm-preserving scheme fails to properly deal with such nearly singular regions, and leaves oscillations after such regions propagate. In sharp contrast to these failures, the proposed scheme keeps working, which shows the superiority of our method. In fact, the method happily works with much coarser spatial and temporal meshes (K=127, $\Delta t=0.1$) for a longer time interval; see Fig. 11. This clearly confirms that the proposed scheme is highly robust also for the subcritical regions. Note that although the proposed scheme does not directly aim at the pulse (solitary wave) solution, as opposed to the integrable systems studies, it successfully captures the pulse solution even at t=1000 (the pulse goes round the spatial interval more than 10 times).

4.3. Numerical experiments for the wave breaking I: periodic case

Next, let us consider more difficult problems where actually singularities can occur—the region including *supercritical* cases.

Following [15], let us consider

$$u_0(x) = a\cos 2\pi x \tag{29}$$

for a fixed parameter a > 0 with the period L = 1. Though the sufficient condition for the wave breaking is a > 1.053, they numerically observed the wave breaking occurs even when a = 0.5 (see, Figures 4 and 5 in [15]). Even though Liu–Pelinovsky–Sakovich did not state how they solved it (since it was a partial differential equation theoretic paper), in order to carry out such simulations very fine meshes, say thousands of spatial grids, are required, and thus generally they are very time-consuming. In such tough regions, our robust scheme becomes much more advantageous.

In our method, for the preparation of the initial condition $\theta_k^{(0)}$, we use $u_{0,x}(x) = -2\pi a \sin 2\pi x$ and the finite difference approximation (19).

As shown in Fig. 12, the numerical result by the proposed scheme is similar to that obtained by Liu-Pelinovsky-Sakovich [15] before the wave breaking. There,

$$\mathcal{B}_{d}(x^{(m)}, u^{(m)}) := \max_{k} u_{k}^{(m)} \frac{u_{k+1}^{(m)} - u_{k-1}^{(m)}}{x_{k+1}^{(m)} - x_{k-1}^{(m)}},$$

is the discrete version of $\mathcal{B}(u(t)) := \sup_{x \in [0,1]} u(x,t) u_x(x,t)$, which diverges at a finite time T_{wb} when the wave breaking occurs (see, [15, Theorem 4]).

Notice that the numerical simulation actually exhibits wave breaking as theoretically suggested even with such a coarse mesh with K=255; this can be seen in the solution u, but is more obvious in terms of θ , which is the argument. The solution exhibits a derivative blow-up when $\theta(\tau,s)$ touches $\pi/2$ at some t and s. The right-bottom panel shows

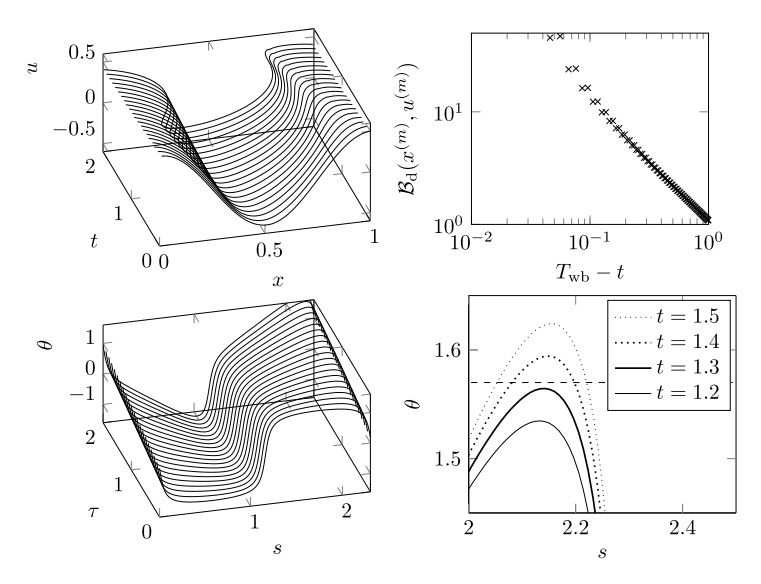


Fig. 12. The numerical solution of the proposed scheme corresponding to the initial condition (29) with a = 0.5 (K = 255, $\Delta t = 0.01$): the top left panel shows the propagation of the numerical solution until t = 2, the top right panel shows the rate of wave breaking ($T_{wb} = 1.356$ is the time of wave breaking computed by Liu–Pelinovsky–Sakovich [15]), the bottom left panel shows the corresponding numerical solution of the SG equation, and its enlarged view is shown in the bottom right panel (the dashed line indicates $\theta = \pi/2$, where the corresponding solution for the SP equation becomes vertical).

the evolution of θ , which actually goes beyond $\pi/2$. Notice again that the proposed scheme is kept robust even such a supercritical case, and thus gives an efficient way of investigating solutions near criticality.

Actually in our regime the solution safely continues even after the wave breaking thanks to the parametrization, which might suggest a possible mathematical way to extend the solution beyond the breaking time (see, Remark 1, and also comments in the concluding remarks).

4.4. Numerical experiments for the wave breaking II: $\mathbb R$ case

We continue the discussion in the previous subsection to further ensure that our robust scheme is useful in blow-up studies. Let us consider another problem setting in [15]; they also considered the \mathbb{R} case, and gave sufficient conditions for global well-posedness and derivative blow-up. They there considered a special initial data

$$u(0, x) = a(1 - 2bx^2)e^{-bx^2}, \quad a > 0, b > 0,$$

and drew a phase diagram in (a, b) space showing the regions of global well-posedness and blow-up; see Figure 3 in [15]. The regions were disjoint, which was consistent with the theory, but between the two regions there remained a wide region for which the theory did not conclude anything. In order to more precisely determine what happens in the unknown region, we must rely on numerical observations.

Our numerical experiments were done in the following way. We consider the problem for b = 1, 2, 3, 4, 5, and tried to determine the critical value of a. In order to replicate \mathbb{R} , sufficiently large computational window was taken; from preliminary test we concluded L = 100 is enough, i.e., under this setting we can ignore the effect of the computational window, and the values at the artificial boundaries are kept close enough to 0 in all the experiments (see the solutions below).

Our scheme is robust enough for all the values of a and b; as mentioned in the previous subsection, it happily works even after singularity occurs. Still, determining the critical value of a is a tough work since the blow-up can be affected by the fineness of the meshes. In the experiments below, we confirmed the accuracy by repeating numerical simulations for a set of (a, b) refining the time and spatial meshes until we can determine $a_{\rm nc}$ with two significant digits.

In Table 1, we listed the following values

- a_{gw} : the value of a given by the sufficient condition for global well-posedness given in [15] (well-posedness is guaranteed for all $a < a_{gw}$),
- $a_{\rm nc}$: the critical value of a numerically observed with the proposed scheme, and
- a_b : the value of a given by the sufficient condition for derivative blow-up given in [15] (blow-up is assured for all $a > a_b$).

Table 1Sufficient conditions and numerical critical values.

b	a_{gw}	$a_{ m nc}$	$a_{\rm b}$
5	0.085	0.39	1.0
4	0.094	0.44	1.1
3	0.11	0.55	1.3
2	0.14	0.61	1.6
1	0.20	0.87	> 2.0

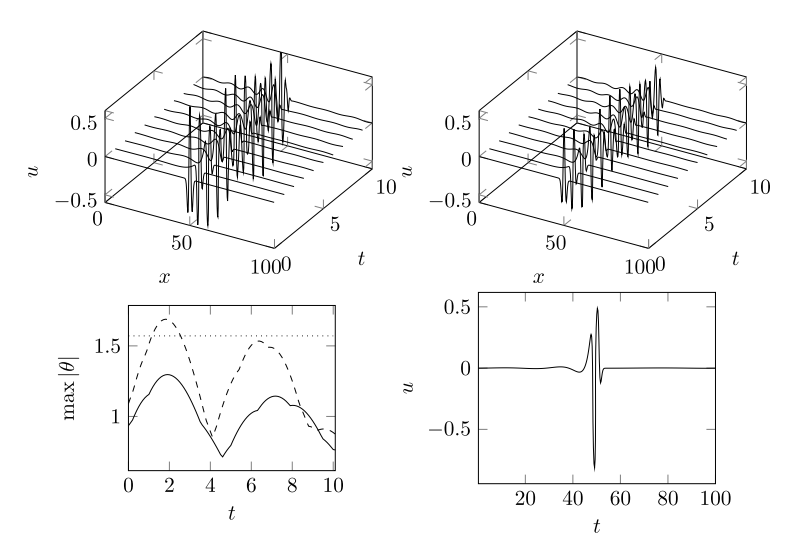


Fig. 13. Numerical results for b=1 (K=401, $\Delta t=0.1$): (top left) the solution for $a=0.70 < a_{\rm nc} \simeq 0.87$, (top right) the solution for $a=1.0 > a_{\rm nc}$, (bottom left) the evolution of $\max_k |\theta_k^{(m)}|$ for a=0.7 (solid line) and a=1.0 (dashed line)—the dotted line shows the blow-up threshold $\theta=\pi/2$, (bottom right) the snapshot at t=2 for $a=1.0 > a_{\rm nc}$.

Obviously they should come in the order $a_{\rm gw} \leq a_{\rm nc} \leq a_{\rm b}$, which actually we observe in Table 1. Notice that the theoretically given sufficient conditions are in fact confirmed numerically, but they are rather conservative. The actual boundary, i.e. the critical value $a_{\rm nc}$, lies in the mid of the values $a_{\rm gw}$ and $a_{\rm b}$. We hope this encourages further theoretical developments.

To illustrate how our scheme works near a criticality, we show the solutions in Fig. 13, which is the case of b=1. The critical value is $a_{\rm nc}\simeq 0.87$, and the figure shows the numerical solutions for the subcritical case a=0.70 and supercritical case a=1.0. From the figure of max $|\theta|$, we see that in fact we see the solution does not exhibit blow-up (at least in the observed time interval) for the former, and it does for the latter. We also see that after the blow-up the solution becomes multi-valued, but after a while it comes back to single-valued; see the discussion in the concluding remarks. The bottom right figure shows a snapshot of the supercritical solution ($a=1.0>a_{\rm nc}$) at b=1.00 at b=1.01 we understand it is after the derivative blow-up and the solution is already multi-valued. Although it is not clearly visible from the figure, we see at least the solution is very steep. In any case, our scheme finds no difficulty in resolving such solutions, which shows the effectiveness of the scheme.

4.5. Numerical examples of multi-valued solutions: the loop and anti-loop solution

In this subsection, let us consider an exotic solution, which is purely multi-valued. Although it does not have any physical meaning itself, we consider it here since not only such exotic solutions are of typical mathematical interest in the short pulse equation studies, but also they give some new insight about the proposed scheme.

Recall in Remark 3 a standard DVDM scheme (21) using the central difference operator was introduced. In our preliminary numerical test, we confirmed that it beautifully reproduced the smooth pulse solution shown in the previous subsection (omitted here.) However, it ceases to work for more difficult cases, and in such a situation, the use of the average-difference method (20) is indispensable. Let us consider the following loop and anti-loop solution

$$\begin{cases} u(\tau, s) = 4\xi \zeta \frac{\xi \sinh \psi \sinh \phi + \zeta \cosh \psi \cosh \phi}{\xi^2 \sinh^2 \psi + \zeta^2 \cosh^2 \phi}, \\ x(\tau, s) = s + 2\xi \zeta \frac{\xi \sinh 2\psi - \zeta \sinh 2\phi}{\xi^2 \sinh^2 \psi + \zeta^2 \cosh^2 \phi}, \end{cases}$$
(30)

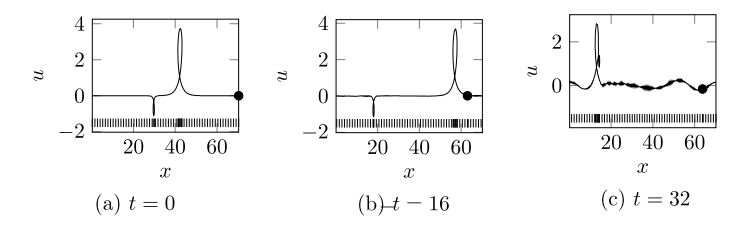


Fig. 14. The loop and anti-loop soliton solution: solid lines correspond to the numerical solution obtained from numerical solution shown in Fig. 15 via discrete hodograph transformation (23) ($\xi = 1.2$, $\Delta t = 0.1$, S = 80, and K = 257). Bars are for every four sample points. The symbol '•' denotes the base point $\left(x_0^{(m)}, u_0^{(m)}\right)$.

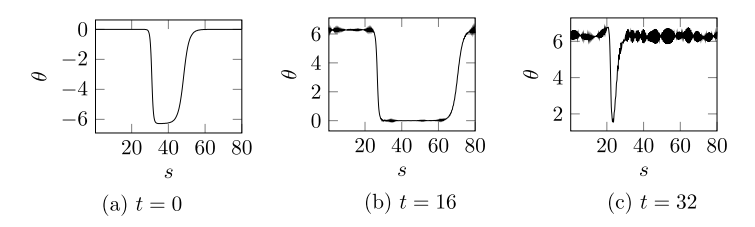


Fig. 15. The loop and anti-loop soliton solution: solid lines correspond to the numerical solutions of the standard DVDM (21) for the SG equation ($\xi = 1.2$, $\Delta t = 0.1$, S = 80, and K = 257).

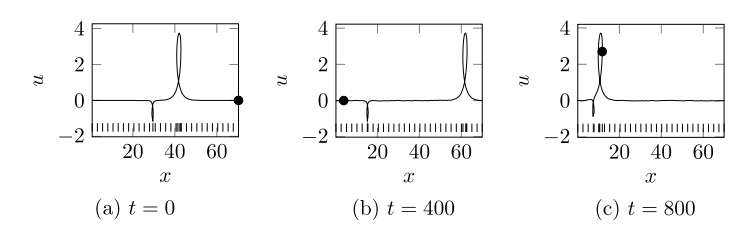


Fig. 16. The loop and anti-loop soliton solution: solid lines correspond to the numerical solution obtained from numerical solution shown in Fig. 17 via the discrete hodograph transformation (23) ($\xi = 1.2$, $\Delta t = 0.1$, S = 80, and K = 129). Bars are for every four sample points. The symbol ' \bullet ' denotes the base point $\left(x_0^{(m)}, u_0^{(m)}\right)$.

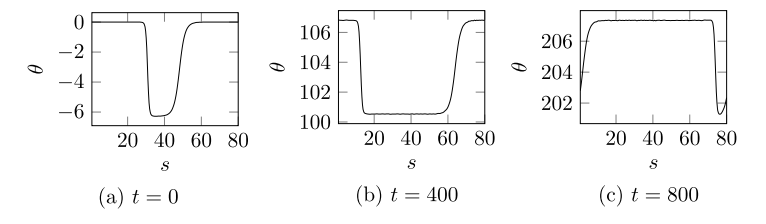


Fig. 17. The loop and anti-loop soliton solution: solid lines correspond to the numerical solutions of the average-difference method (20) for the SG equation ($\xi = 1.2$, $\Delta t = 0.1$, S = 80, and K = 129).

where the parameter $\xi > 1$, $\phi = \xi(s + \tau)$, $\psi = \zeta(s - \tau)$, $\zeta = \sqrt{\xi^2 - 1}$. Again, in what follows, we employed the finite difference approximation (19) for preparing the initial data.

As shown in Figs. 14 and 15, the standard DVDM (21) cannot reproduce the loop and anti-loop solution with $\xi = 1.2$ under the condition $\Delta t = 0.1$, S = 80, and K = 257. On the other hand, even if we employ larger mesh sizes K = 129, the proposed scheme reproduces the solution until t = 800 as shown in Figs. 16 and 17. The bars in Fig. 16 denote the grids; we can observe that the grids become dense around the loop and anti-loop solutions, which reflects the moving mesh property of the proposed scheme. The bold circle " \bullet " denotes the base point (recall (10) for the continuous case, and (25a) and (25b) for the discrete case). It is observed that the base point moves as time goes by (which is demanded in the periodic case), and furthermore, the solution is successfully continuous around that point.

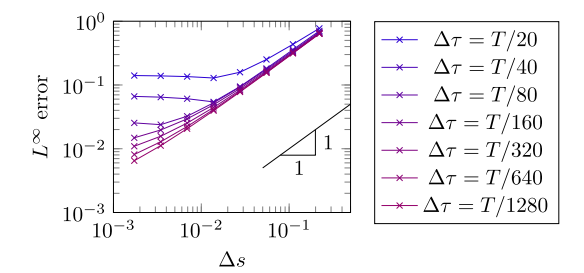


Fig. 18. L^{∞} errors of the proposed scheme with respect to Δs for each step size $\Delta \tau$.

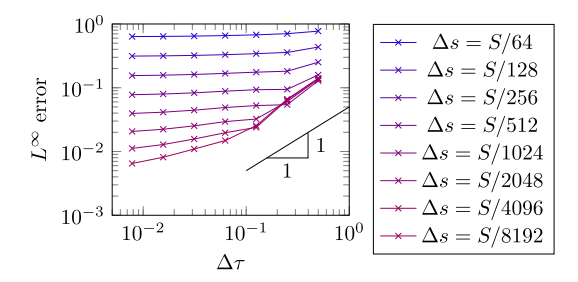


Fig. 19. L^{∞} errors of the proposed scheme with respect to $\Delta \tau$ for each mesh size Δs .

4.6. Error behavior

In this subsection, to see the error behavior of the proposed scheme, we use an exact solution on the periodic domain devised by Parkes [23] (see also Matsuno [24] for similar periodic solutions). One of the periodic traveling-wave solutions can be written as follows:

$$\begin{cases} x(\tau, s) = v\tau + x_0 - s + \frac{1}{\alpha^2}\tau + \frac{2}{\alpha}E\left(\alpha s - \frac{\tau}{\alpha} \mid \xi\right), \\ u(\tau, s) = \pm \frac{2\sqrt{\xi}}{\alpha}\operatorname{cn}\left(\alpha s - \frac{\tau}{\alpha} \mid \xi\right), \end{cases}$$
(31)

where v>0 represents the velocity of the traveling-wave, $\xi\in(0,1/2)$ denotes the parameter related to the shape of the wave, and $\alpha:=\sqrt{(1-2\xi)/v}$. Here, $\operatorname{cn}(w|\xi)$ is a Jacobian elliptic function, and $E(w|\xi)$ is the elliptic integral of the second kind (with the notation as in [54]). We also use the Jacobian elliptic functions $\operatorname{sn}(w|\xi)$ and $\operatorname{dn}(w|\xi)$ below. In the numerical simulation, we employ $v=1, x_0=0$, and $\xi=0.25$ ($S\approx19.072$).

The corresponding solution of the SG equation is given by

$$\theta(\tau, s) = \arctan \frac{\mp 2\sqrt{\xi} \operatorname{sn}\left(\alpha s - \frac{\tau}{\alpha} \mid \xi\right) \operatorname{dn}\left(\alpha s - \frac{\tau}{\alpha} \mid \xi\right)}{-1 + 2\left(\operatorname{dn}\left(\alpha s - \frac{\tau}{\alpha} \mid \xi\right)\right)^{2}}.$$
(32)

We computed $\theta^{(0)}$ from this expression to prepare accurate initial data to capture the exact solution.

As shown in Figs. 18 and 19, the L^{∞} errors at the fixed time T=10 decay in the order $O(\Delta s + \Delta \tau)$. Here, the L^{∞} error in the physical domain is defined as $\sup_{s \in \mathbb{R}} |u(T,s) - \tilde{u}_T(x(T,s))|$, where $\tilde{u}_T : \mathbb{R} \to \mathbb{R}$ is the linear interpolation of the numerical solution $(x_k^{(M)}, u_k^{(M)})$ at the final step. Strictly speaking, since the computation of the exact L^{∞} error is not easy due to the complicated expression (31) of the exact solution, instead we use a fine (with 100 K sample points) piecewise linear interpolation of the exact solution.

5. Concluding remarks

In this paper, we established a new robust numerical scheme for the short pulse equation, employing several ideas from integrable systems, moving mesh methods, and structure-preserving methods; none of which is truly dispensable. We hope that, in the reverse direction, this work will invoke new discussions in each research field. Through various numerical experiments we confirmed that the proposed scheme is in fact quite robust, and useful for investigating solution behaviors near criticality. In fact, by utilizing the scheme some derivative blow-up phenomena have been numerically investigated, and several new insights have been obtained, including the precise critical values which have been left uninvestigated in a preceding study. An interesting finding is that, as shown in Fig. 13, solution of the short pulse equation can once

go beyond the singularity and become multi-valued, and after a while, it can come back; of course this is only when we admit such multi-valued solutions as solutions of the original short pulse equation in a generalized sense. This direction of extending solution is, however, already suggested in some studies, for example, in [55]. The proposed scheme and the regime on which the scheme is based on might be useful in such a research direction.

Some possible future works are in order. Feng–Maruno–Ohta [40] showed that the short pulse equation is also associated with the coupled dispersionless (CD) equation [56,57], and this relation can be used for the construction of another robust numerical integrator. The present authors have already confirmed that a numerical scheme can be constructed based on this formulation [58]. The advantage of this is that, although the present study has made full use of the features of the short pulse equation, the method based on the CD formulation is less restrictive, and thus can be applied to wider range of partial differential equations (PDEs) including the complex SP equation, whose exact solutions were recently found by Ling–Feng–Zhu [59]. Another interesting topic is, as stated in Introduction, the challenge of extending standard moving mesh methods directly to the PDEs including the term u_{ix} .

Acknowledgments

This work was partly supported by JSPS KAKENHI Grant Numbers 25287030, 15H03635, 16KT0016, and 17H02826, JST CREST Grant Number JPMJCR14D2, Japan, NSF Grant No. DMS-1715991 of United States, and National Natural Science Foundation of China under Grant No. 11728103. The first author is supported by the Research Fellowship of the Japan Society for the Promotion of Science for Young Scientists, Japan. The authors are grateful to the anonymous referee's comments.

Appendix. Properties of the norm-preserving scheme in Section 4.1

Here we show some properties of the norm-preserving scheme devised in Section 4.1. First, we note that the solutions of (26) preserve "mass".

Lemma 12. Let $\overline{u}_k^{(m)}$ be the numerical solution of the scheme (26) under the periodic boundary condition and initial condition satisfying $\sum_k \overline{u}_k^{(0)} = 0$. Then, $\sum_{k=1}^K \overline{u}_k^{(m)} \Delta x = 0$ holds for all m = 0, 1, ..., M.

Thanks to the lemma above, and by using the relation $\delta_x^+ \delta_{FD}^{-1} = \delta_{FD}^{-1} \delta_x^+ = \mu_x^+$ for zero-mean vectors which can be proved in a straight forward manner (see, [43]), the numerical scheme (26) is shown to be equivalent to (27). In order to prove Proposition 11, the skew-symmetry of the discrete antiderivative δ_{FD}^{-1} is important.

Lemma 13 ([47, Lemma 6]). For any N-periodic sequences v, w such that satisfy $\sum_k v_k = \sum_k w_k = 0$, it holds that $\sum_{k=1}^N v_k \delta_{\text{FD}}^{-1} v_k + \sum_{k=1}^N w_k \delta_{\text{FD}}^{-1} v_k = 0$. In particular, $\sum_{k=1}^N v_k \delta_{\text{FD}}^{-1} v_k = 0$ holds.

Proof. By summing up (26) for $k=1,\ldots,K$, we see $\delta_t^+\sum_{k=1}^K\overline{u}_k^{(m)}=0$. This implies the lemma due to the assumption $\sum_k\overline{u}_k^{(0)}=0$.

Then the proof of Proposition 11 reads as follows.

Proof. For the numerical solution $\overline{u}_k^{(m)}$ of the scheme (26), we see

$$\begin{split} \delta_{t}^{+}\overline{\mathcal{I}}_{d}\left(\overline{u}^{(m)}\right) &= \sum_{k=1}^{K} \left(\mu_{t}^{+}\overline{u}_{k}^{(m)}\right) \left(\delta_{t}^{+}\overline{u}_{k}^{(m)}\right) \Delta x \\ &= \sum_{k=1}^{K} \left(\mu_{t}^{+}\overline{u}_{k}^{(m)}\right) \left(\delta_{\text{FD}}^{-1}\mu_{t}^{+}\overline{u}_{k}^{(m)} + \frac{1}{6}\delta_{x}^{-} \left(\left(\mu_{x}^{+} \left(\mu_{t}^{+}\overline{u}_{k}^{(m)}\right)^{2}\right)\mu_{x}^{+}\mu_{t}^{+}\overline{u}_{k}^{(m)}\right)\right) \Delta x \\ &= -\frac{1}{6}\sum_{k=1}^{K} \left(\delta_{x}^{+}\mu_{t}^{+}\overline{u}_{k}^{(m)}\right) \left(\left(\mu_{x}^{+} \left(\mu_{t}^{+}\overline{u}_{k}^{(m)}\right)^{2}\right)\mu_{x}^{+}\mu_{t}^{+}\overline{u}_{k}^{(m)}\right) \Delta x \\ &= -\frac{1}{12}\sum_{k=1}^{K} \left(\delta_{x}^{+} \left(\mu_{t}^{+}\overline{u}_{k}^{(m)}\right)^{2}\right) \left(\mu_{x}^{+} \left(\mu_{t}^{+}\overline{u}_{k}^{(m)}\right)^{2}\right) \Delta x \\ &= -\frac{1}{24}\sum_{k=1}^{K} \delta_{x}^{+} \left(\mu_{t}^{+}\overline{u}_{k}^{(m)}\right)^{4} \Delta x = 0. \end{split}$$

Here, third equality comes from the skew-symmetry of $\delta_{\rm FD}^{-1}$ (recall that $\mu_t^+ \overline{u}^{(m)}$ is a zero-mean vector due to Lemma 12) and the summation-by-parts formula with respect to $\delta_{\rm x}^-$ (see e.g. [45]). \Box

References

- [1] T. Schäfer, C.E. Wayne, Propagation of ultra-short optical pulses in cubic nonlinear media, Physica D 196 (1–2) (2004) 90–105, http://dx.doi.org/10.1016/j.physd.2004.04.007.
- [2] Y. Chung, C.K.R.T. Jones, T. Schäfer, C.E. Wayne, Ultra-short pulses in linear and nonlinear media, Nonlinearity 18 (3) (2005) 1351–1374, http://dx.doi.org/10.1088/0951-7715/18/3/021.
- [3] J.C. Brunelli, The short pulse hierarchy, J. Math. Phys. 46 (12) (2005) 123507, 9, http://dx.doi.org/10.1063/1.2146189.
- [4] J.C. Brunelli, The bi-Hamiltonian structure of the short pulse equation, Phys. Lett. A 353 (6) (2006) 475–478, http://dx.doi.org/10.1016/j.physleta. 2006.01.009.
- [5] A. Sakovich, S. Sakovich, The short pulse equation is integrable, J. Phys. Soc. Japan 74 (1) (2005) 239–241, http://dx.doi.org/10.1143/JPSJ.74.239, URL http://journals.jps.jp/doi/pdf/10.1143/JPSJ.74.239.
- [6] A. Sakovich, S. Sakovich, Solitary wave solutions of the short pulse equation, J. Phys. A 39 (22) (2006) L361–L367, http://dx.doi.org/10.1088/0305-4470/39/22/L03.
- [7] Y. Matsuno, Multiloop soliton and multibreather solutions of the short pulse model equation, J. Phys. Soc. Japan 76 (8) (2007) 084003, URL http://dx.doi.org/10.1143/JPSJ.76.084003.
- [8] E.J. Parkes, S. Abbasbandy, Finding the one-loop soliton solution of the short-pulse equation by means of the homotopy analysis method, Numer. Methods Partial Differential Equations 25 (2) (2009) 401–408, http://dx.doi.org/10.1002/num.20348.
- [9] H. Liu, J. Li, Lie symmetry analysis and exact solutions for the short pulse equation, Nonlinear Anal. 71 (5-6) (2009) 2126-2133, http://dx.doi.org/10.1016/j.na.2009.01.075.
- [10] Z. Fu, Z. Chen, L. Zhang, J. Mao, S. Liu, Novel exact solutions to the short pulse equation, Appl. Math. Comput. 215 (11) (2010) 3899–3905, http://dx.doi.org/10.1016/j.amc.2009.11.038.
- [11] G. Gambino, U. Tanriver, P. Guha, A.G. Choudhury, S.R. Choudhury, Regular and singular pulse and front solutions and possible isochronous behavior in the short-pulse equation: phase-plane, multi-infinite series and variational approaches, Commun. Nonlinear Sci. Numer. Simul. 20 (2) (2015) 375–388, http://dx.doi.org/10.1016/j.cnsns.2014.06.011.
- [12] D. Pelinovsky, A. Sakovich, Global well-posedness of the short-pulse and sine-Gordon equations in energy space, Comm. Partial Differential Equations 352 (4) (2010) 613–629, http://dx.doi.org/10.1080/03605300903509104.
- [13] G.M. Coclite, L. di Ruvo, Well-posedness results for the short pulse equation, Z. Angew. Math. Phys. 66 (4) (2015) 1529–1557, http://dx.doi.org/10.1007/s00033-014-0478-6.
- [14] G.M. Coclite, J. Ridder, N.H. Risebro, A convergent finite difference scheme for the Ostrovsky-Hunter equation on a bounded domain, BIT 57 (1) (2017) 93–122, http://dx.doi.org/10.1007/s10543-016-0625-x.
- [15] Y. Liu, D. Pelinovsky, A. Sakovich, Wave breaking in the short-pulse equation, Dyn. Partial Differ. Equ. 6 (4) (2009) 291–310, http://dx.doi.org/10.4310/DPDE.2009.v6.n4.a1.
- [16] A. Sakovich, Well-posedness of Nonlinear Wave Equations in Characteristic Coordinates (Master's thesis), McMaster University, 2009.
- [17] M. Pietrzyk, I. Kanattšikov, U. Bandelow, On the propagation of vector ultra-short pulses, J. Nonlinear Math. Phys. 15 (2) (2008) 162–170, http://dx.doi.org/10.2991/jnmp.2008.15.2.4.
- [18] N. Costanzino, V. Manukian, C.K.R.T. Jones, Solitary waves of the regularized short pulse and Ostrovsky equations, SIAM J. Math. Anal. 41 (5) (2009) 2088–2106, http://dx.doi.org/10.1137/080734327.
- [19] B.-F. Feng, An integrable coupled short pulse equation, J. Phys. A 45 (8) (2012) 085202, http://dx.doi.org/10.1088/1751-8113/45/8/085202, 14.
- [20] L. Kurt, Y. Chung, T. Schäfer, Higher-order corrections to the short-pulse equation, J. Phys. A 46 (28) (2013) 285205, 13, http://dx.doi.org/10. 1088/1751-8113/46/28/285205.
- [21] L. Kurt, T. Schäfer, Propagation of ultra-short solitons in stochastic Maxwell's equations, J. Math. Phys. 55 (1) (2014) 011503, 11, http://dx.doi.org/10.1063/1.4859815.
- [22] B.-F. Feng, Complex short pulse and coupled complex short pulse equations, Physica D 297 (2015) 62–75, http://dx.doi.org/10.1016/j.physd. 2014.12.002.
- [23] E.J. Parkes, Some periodic and solitary travelling-wave solutions of the short-pulse equation, Chaos Solitons Fractals 38 (1) (2008) 154–159, http://dx.doi.org/10.1016/j.chaos.2006.10.055.
- [24] Y. Matsuno, Periodic solutions of the short pulse model equation, J. Math. Phys. 49 (7) (2008) 073508, 18, http://dx.doi.org/10.1063/1.2951891.
- [25] Y. Shen, F. Williams, N. Whitaker, P. Kevrekidis, A. Saxena, D. Frantzeskakis, On some single-hump solutions of the short-pulse equation and their periodic generalizations, Phys. Lett. A 374 (29) (2010) 2964–2967, http://dx.doi.org/10.1016/j.physleta.2010.05.014.
- [26] M. Pietrzyk, I. Kanattšikov, On the polysymplectic integrator for the short pulse equation (December 2015). arXiv:1512.09105.
- [27] S. Amiranashvili, A.G. Vladimirov, U. Bandelow, Solitary-wave solutions for few-cycle optical pulses, Phys. Rev. A 77 (2008) 063821, http://dx.doi.org/10.1103/PhysRevA.77.063821, URL https://link.aps.org/doi/10.1103/PhysRevA.77.063821.
- [28] H. Leblond, D. Mihalache, Few-optical-cycle solitons: Modified Korteweg-de Vries sine-Gordon equation versus other non-slowly-varying-envelope-approximation models, Phys. Rev. A 79 (2009) 063835, http://dx.doi.org/10.1103/PhysRevA.79.063835, URL https://link.aps.org/doi/10.1103/PhysRevA.79.063835.
- [29] H. Leblond, D. Mihalache, Models of few optical cycle solitons beyond the slowly varying envelope approximation, Phys. Rep. 523 (2) (2013) 61–126, http://dx.doi.org/10.1016/j.physrep.2012.10.006.
- [30] M. Kolesik, J.V. Moloney, Modeling and simulation techniques in extreme nonlinear optics of gaseous and condensed media, Rep. Prog. Phys. 77 (1) (2014) 016401, URL http://stacks.iop.org/0034-4885/77/i=1/a=016401.
- [31] W. Huang, R.D. Russell, Adaptive Moving Mesh Methods, in: Applied Mathematical Sciences, vol. 174, Springer, New York, 2011, p. xviii+432, http://dx.doi.org/10.1007/978-1-4419-7916-2.
- [32] C.J. Budd, W. Huang, R.D. Russell, Adaptivity with moving grids, Acta Numer. 18 (2009) 111-241, http://dx.doi.org/10.1017/S0962492906400015.
- [33] T.P. Horikis, The short-pulse equation and associated constraints, J. Phys. A 42 (44) (2009) 442004, http://dx.doi.org/10.1088/1751-8113/42/44/442004, 5.
- [34] B.-F. Feng, J. Inoguchi, K. Kajiwara, K. Maruno, Y. Ohta, Discrete integrable systems and hodograph transformations arising from motions of discrete plane curves, J. Phys. A 44 (2011) 395201, http://dx.doi.org/10.1088/1751-8113/44/39/395201, (19pp). URL http://stacks.iop.org/1751-8121/44/i=39/a=395201.
- [35] M. Wadati, K. Konnno, Y. Ichikawa, New integrable nonlinear evolution equations, J. Phys. Soc. Japan 47 (5) (1979) 1698–1700, http://dx.doi.org/10.1143/JPSJ.47.1698.
- [36] B.-F. Feng, K. Maruno, Y. Ohta, Integrable discretizations for the short-wave model of the Camassa-Holm equation, J. Phys. A 43 (26) (2010) 265202, http://dx.doi.org/10.1088/1751-8113/43/26/265202, (14pp).
- [37] B.-F. Feng, K. Maruno, Y. Ohta, Integrable discretizations of the short pulse equation, J. Phys. A 43 (8) (2010) 085203, http://dx.doi.org/10.1088/1751-8113/43/8/085203, (14pp).

- [38] B.-F. Feng, K. Maruno, Y. Ohta, A self-adaptive moving mesh method for the Camassa-Holm equation, J. Comput. Appl. Math. 235 (1) (2010) 229–243, http://dx.doi.org/10.1016/j.cam.2010.05.044.
- [39] Y. Ohta, K. Maruno, B.-F. Feng, An integrable semi-discretization of the Camassa-Holm equation and its determinant solution, J. Phys. A 41 (35) (2008) 355205, http://dx.doi.org/10.1088/1751-8113/41/35/355205, (30pp).
- [40] B.-F. Feng, K. Maruno, Y. Ohta, Self-adaptive moving mesh schemes for short pulse type equations and their Lax pairs, Pac. J. Math. Ind. 6 (2014) Art. 8. 14. http://dx.doi.org/10.1186/s40736-014-0008-7.
- [41] B.-F. Feng, J. Chen, Y. Chen, K.-i. Maruno, Y. Ohta, Integrable discretizations and self-adaptive moving mesh method for a coupled short pulse equation, J. Phys. A 48 (38) (2015) 385202, 21, http://dx.doi.org/10.1088/1751-8113/48/38/385202.
- [42] J.K. Hunter, Numerical solutions of some nonlinear dispersive wave equations, in: Computational Solution of Nonlinear Systems of Equations (Fort Collins, CO, 1988), in: Lectures in Appl. Math., vol. 26, Amer. Math. Soc., Providence, RI, 1990, pp. 301–316.
- [43] S. Sato, T. Matsuo, On spatial discretization of evolutionary differential equations on the periodic domain with a mixed derivative, J. Comput. Appl. Math. 358 (2019) 221–240. http://dx.doi.org/10.1016/j.cam.2019.03.021.
- [44] D. Furihata, Finite difference schemes for $\partial u/\partial t = (\partial/\partial x)^{\alpha} \delta G/\delta u$ that inherit energy conservation or dissipation property, J. Comput. Phys. 156 (1) (1999) 181–205, http://dx.doi.org/10.1006/jcph.1999.6377.
- [45] D. Furihata, T. Matsuo, Discrete Variational Derivative Method-A Structure-preserving Numerical Method for Partial Differential Equations, CRC Press. Boca Raton, 2011.
- [46] Y. Miyatake, T. Yaguchi, T. Matsuo, Numerical integration of the Ostrovsky equation based on its geometric structures, J. Comput. Phys. 231 (14) (2012) 4542–4559, http://dx.doi.org/10.1016/j.jcp.2012.02.027.
- [47] T. Yaguchi, T. Matsuo, M. Sugihara, Conservative numerical schemes for the Ostrovsky equation, J. Comput. Appl. Math. 234 (4) (2010) 1036–1048, http://dx.doi.org/10.1016/j.cam.2009.03.008.
- [48] D. Furihata, S. Sato, T. Matsuo, A novel discrete variational derivative method using "average-difference methods", JSIAM Lett. 8 (2016) 81–84, http://dx.doi.org/10.14495/jsiaml.8.81.
- [49] H. Kanazawa, T. Matsuo, T. Yaguchi, A conservative compact finite difference scheme for the KdV equation, JSIAM Lett. 4 (2012) 5-8, http://dx.doi.org/10.14495/jsiaml.4.5.
- [50] B. Fornberg, A Practical Guide to Pseudospectral Methods, in: Cambridge Monographs on Applied and Computational Mathematics, vol. 1, Cambridge University Press, Cambridge, 1996, p. x+231, http://dx.doi.org/10.1017/CB09780511626357.
- [51] K. Oguma, Construction of Moving Mesh Finite Difference Schemes for PDEs via Hodograph Transformation (in Japanese) (Master's thesis), The University of Tokyo. 2014.
- [52] T.J. Bridges, S. Reich, Multi-symplectic integrators: numerical schemes for Hamiltonian PDEs that conserve symplecticity, Phys. Lett. A 284 (4–5) (2001) 184–193, http://dx.doi.org/10.1016/S0375-9601(01)00294-8.
- [53] B. Moore, S. Reich, Backward error analysis for multi-symplectic integration methods, Numer. Math. 95 (4) (2003) 625–652, http://dx.doi.org/ 10.1007/s00211-003-0458-9
- [54] M. Abramowitz, I.A. Stegun, Handbook of Mathematical Functions with Formulas, Graphs, and Mathematical Tables, in: National Bureau of
- Standards Applied Mathematics Series, vol. 55, U.S. Government Printing Office, Washington, D.C., 1964, p. xiv+1046.
 [55] A. Boutet de Monvel, D. Shepelsky, L. Zielinski, The short pulse equation by a Riemann-Hilbert approach, Lett. Math. Phys. 107 (7) (2017)
- 1345–1373, http://dx.doi.org/10.1007/s11005-017-0945-z. [56] K. Konno, H. Oono, New coupled integrable dispersionless equations, J. Phys. Soc. Japan 63 (2) (1994) 377–378, http://dx.doi.org/10.1143/JPSJ.
- 63.377.

 [57] R. Hirota, S. Tsujimoto, Note on "New coupled integrable dispersionless equations", J. Phys. Soc. Japan 63 (9) (1994) 3533–3534, http://dx.doi.org/10.1143/[PS].63.3533, URL http://journals.jps.jp/doi/pdf/10.1143/[PS].63.3533.
- [58] S. Sato, T. Matsuo, B.-F. Feng, A norm-preserving self-adaptive moving mesh integrator for the short pulse equation, RIMS Kokyuroku 1995 (2016) 82–91, URL http://www.kurims.kyoto-u.ac.jp/~kyodo/kokyuroku/contents/pdf/1995-12.pdf.
- [59] L. Ling, B.-F. Feng, Z. Zhu, Multi-soliton, multi-breather and higher order rogue wave solutions to the complex short pulse equation, Physica D 327 (2016) 13–29, http://dx.doi.org/10.1016/j.physd.2016.03.012.